Journal of Materials Research and Technology 39 (2025) 7588–7612

Contents lists available at ScienceDirect

Journal of Materials Research and Technology

journal homepage: www.elsevier.com/locate/jmrt

Experimental investigation of the tensile properties of steel foam hollow sphere assemblies

Thomas Kalpakoglou [a,*], Georgios Constantinides [b], Stylianos Yiatros [a]

[a] Department of Civil Engineering and Geomatics, Cyprus University of Technology, Limassol, Cyprus
[b] Department of Mechanical Engineering and Materials Science and Engineering, Cyprus University of Technology, Limassol, 3036, Cyprus

ARTICLE INFO

Keywords:
Metal foam
Steel foam hollow sphere assemblies
Tensile loading
Elastic modulus
Tensile strength
Scanning electron microscopy (SEM)

ABSTRACT

The present research aims to study the mechanical properties of steel foam hollow sphere assemblies of various relative densities under the effect of uniaxial tensile loading, evaluating the validity of a new test protocol and comparing it with other experimental results. Through a series of experiments with different groups of specimens, which were recorded step by step, the effects of factors such as the relative density and the number of bonds on the mechanical properties of the specimens were identified, and their impact on the response discussed. The shape of the specimen is cubic with dimensions 50 × 50 × 50 mm^3. The range of values recorded in this research for the Elastic Modulus is 340,89–399,28 MPa, and for Tensile Strength is 2,8-3,53 MPa, as exhibited by the five different groups of specimens tested in the present study with relative density from 0,059 to 0,074. The promising experimental results support the proposed methodology and test protocol for studying similar assemblies under tensile loading and an attempt to explain the differences between past scaling equations and experimental results. Scanning electron microscopy (SEM) is also performed and presented to examine the microstructure of the specimens and the crack surface.

1. Introduction

Metal foams and metal foam sphere assemblies are the subject of several publications on the investigation of the mechanical behaviour of foams and how this relates to their structure [2–5]. This is due to the large number of potential applications for metal foams in various industrial sectors [6–12]. More specifically, metal foams find application in the following sectors: automotive industry [13–16], shipbuilding industry [17,18],aerospace industry[19–22], chemical industry [23–27], building construction [28–34],energy storage [35–39], bio-medical [40–46].

These industrial applications often involve complex loading conditions, where compressive, tensile, and shear forces are present, such as vehicle crash energy absorbers [47], structural supports in aerospace engineering [48], or load-bearing orthopaedic implants [49]. However, the lack of reliable data and testing protocols for tensile behaviour limits the integration of metal foams into critical components where failure under tension could be catastrophic. Understanding the tensile properties of metal foam structures is thus essential for their broader adoption in engineering design, particularly in applications where lightweight and high-strength materials are required under multidirectional loads. For example, understanding how materials respond to tension is essential in automotive interiors, as it significantly influences the safety, longevity, and overall performance of the vehicle's interior parts [50] or identifying how implant materials react to stretching is vital for guaranteeing their durability and stability over time within the body[51]. Recognising tensile strength and elastic modulus is crucial for ensuring structural integrity and durability [52].

However, a significant proportion of these works focuses on the compressive properties of these materials [1,53–55], a reasonable outcome due to the beneficial metal foam attribute for energy absorption [56–58]. Although some works for other loading scenarios exist [59–63]and have been meticulously mapped in Kalpakoglou and Yiatros [95] concerning tensile and shear properties, it is essential to explore reliable testing protocols for other archetypal mechanical properties of metal foams under such loading scenarios [64–66].

Metal foams comprising hollow spheres are characterised by good energy absorption, high strength, heat storage, and low density [67–72]. These foams have a certain volume fraction of closed pore space within the spheres and a pore space between the assembled spheres, whether sintered or bonded via other means. The metal foam hollow spheres can be produced by injecting a metal hydride solution through a specially designed nozzle [73–75]. This method takes advantage of surface

* Corresponding author.
E-mail address: tx.kalpakoglou@edu.cut.ac.cy (T. Kalpakoglou).

https://doi.org/10.1016/j.jmrt.2025.11.036
Received 28 April 2025; Received in revised form 22 October 2025; Accepted 5 November 2025
Available online 7 November 2025

List of abbreviations and symbols

SHS2	Specimen with purely 2 mm spheres, as defined in Yiatros et al. [1]
SHS4	Specimen with purely 4 mm spheres, as defined in Yiatros et al. [1]
SHS2_0,75_SHS4_0,25	Specimen with 75 % 2 mm spheres and 25 % 4 mm spheres, by volume
SHS2_0,5_SHS4_0,5	Specimen with 50 % 2 mm spheres and 50 % 4 mm spheres, by volume
SHS2_0,25_SHS4_0,75	Specimen with 25 % 2 mm spheres and 75 % 4 mm spheres, by volume
SEM	Scanning Electron Microscopy
L:	Length of specimen
W	Width of specimen
H	Height of specimen
ρ :	Specimen density
ρ_s	Density of solid steel
E:	Elastic Modulus
E_s:	Elastic modulus of steel
σ_{max} :	Tensile strength
σ_{ys}:	Tensile strength of steel
ρ/ρ_s:	Relative density
E/E_s:	Relative Elastic modulus
σ_{max}/σ_{ys}:	Relative Tensile strength

tension phenomena to generate spherical shapes. Another method involves spraying styrofoam spheres with a metal hydride solution [76,77]. The resulting spheres can then be bonded together, creating a solid structure with relatively low porosity, with a resin or molten metal with a low melting point (aluminium or magnesium) covering the intermediate spaces between the spheres. Another way to bond spheres together involves spraying them with some binder or low-point metal, melting and welding them while the connecting material is still liquid. Alternatively, sintering can be applied with simultaneous isostatic compression to bond spheres through diffusion. However, through this method, the walls of the spheres distort at the adjoining points [78–80]. Various studies have also been carried out on the effect of sintering temperature on their properties, revealing the extent of their influence as they lead to different properties [81].

Friedl et al. [82] explored the impact of density and structure on the behaviour of hollow sphere metal foams subjected to tensile loading. Their findings revealed increased density resulted in the specimens' more substantial ultimate tensile strength. Similarly, Szyniszewski et al. [83] examined hollow sphere specimens exhibiting limited ductility. A steel plate was inserted into a notch on the specimen to facilitate load transfer to the specimen. The fracture typically occurred in the region connecting the spheres. They also found that larger diameter spheres positively influenced the overall strength of the specimens without altering their density.

Vealy (2010) [98] examined specimens with varying pore densities (20 ppi and 40 ppi) and relative densities between 6 and 8 %, focusing on their mechanical properties. He emphasised the considerable discrepancy between the experimental findings for the elasticity modulus and the theoretical predictions made by Gibson and Ashby [84]. He attributed this difference to porosity and ligament geometry variations between the different pore structures. Zimar et al. [85] studied the non-linear response of metal foams under tensile stress using finite element analysis and compared their simulation results with the experimental data from Vealy (2010) [98]. They observed a higher stress at the same strain than the experimental results. Additionally, the Elastic Modulus was greater than the theoretical values predicted by Gibson and Ashby [84] through scaling equations.

Foroughi et al. [86] conducted a study on closed-cell foam known by the trade name Alulight. They developed exported models suitable for finite element method (FEM) analysis to predict the mechanical properties of cellular materials, including structures composed of hollow spheres or fibre architectures. Their work provides valuable insights into the structural behaviour of such advanced materials, facilitating the design and optimisation of lightweight, high-performance cellular structures. Marx and Rabiei [87] investigated two specimen versions and identified differences in their fracture areas. To prevent uniaxial loading caused by improper specimen positioning—specifically, specimens not being properly centred—they employed aluminium spacers on the grips to ensure accurate centring during testing. Vengatachalam et al. [88] examined Alporas, a type of closed-cell foam, at two distinct relative densities—11.7 % and 17.2 %—under various loading conditions. Notable variations were identified in the deformation behaviours of the samples when subjected to tensile and compressive forces. They introduced an initial performance metric for closed-cell foams, tailored explicitly to closed-cell aluminium foams, which effectively captures the asymmetric characteristics of the yield surface relative to the active stress axis. This criterion relies solely on the uniaxial compressive strength parameter.

Qing et al. [89] studied iron metal foam, concentrating on developing an efficient bonding technique between the foam and the metal face. They employed a custom setup that included a stainless-steel plate in contact with the specimen, connected via a steel rod with grips to facilitate the experiments. Bolzoni et al. [90] investigated both Fe + NaCl and Ti + NaCl open and closed cell foams. They found that Fe foam demonstrates superior elastoplastic behaviour compared to Ti, which exhibits pseudoplastic characteristics. The authors concluded that empirical models are insufficient for accurately predicting the overall behaviour of general foams. Conversely, structural-analytical models can provide satisfactory predictions for specific mechanical properties, such as elasticity, considering a particular pore volume. In summary, they developed new models aimed at more accurately and efficiently calculating the mechanical properties of foams.

McCullough et al. [91] examined a closed-cell foam known by the trade name Alulight. Their findings indicate that the foam exhibits contrasting responses when subjected to compression and tension: it behaves semi-brittly under tensile stress, whereas it demonstrates ductile characteristics under compression—this type of foam shares several properties with open-cell foams. Prior research [92] analysed crack growth within the same material and emphasised the beneficial impact of higher density in enhancing plane strain fracture toughness and the unloading modulus. Motz and Pippan [93] validate the contrasting response of metal foam under tensile stress compared to compression loading, studying closed-cell foam at two different densities (0.25 g/cm^3 and 0.40 g/cm^3). No deformation bands were observed, apart from during the ultimate failure. Wang et.al. [94]. highlight the different behaviour, deformation, and fracture mechanics between tension and compression. Specimens did not show the deformation band except for the final failure. Also, their loading and unloading modulus results confirm the conclusions of McCullough et al. [91]. Kashef et al. [96] observed that higher-density specimens show more considerable strength.

Table 1 includes summarised information for the physical properties of the foams, such as the density and relative density, and the observed mechanical properties from the mentioned research works.

Despite the growing interest in metal foams, there is still a notable lack of standardised protocols and consistent data on their tensile performance. This gap significantly hinders predictive modelling and safe design of foam-based components subjected to tensile or combined loading conditions. The present research aims to explore reliable specimen preparation and testing protocols for metal foams and metal foam sphere assemblies, drawing inspiration from set ups pertinent to flatwise tensile tests for adhesives and investigate whether the use of a sufficiently strong adhesive could shift the failure inside the specimen and

Table 1
Mechanical properties of foams from previous research [95].

Title	Material	Density	Relative Density	Elastic Modulus	Tensile Strength	Relative Elastic modulus
Tensile and shear properties of aluminium foam [94]	Aluminium	–	0,09	106,3 MPa	3,94 MPa	1,54 x 10^{-3}
Uniaxial stress-strain behaviour of aluminum alloy foams [91]	Aluminium	0,65	0,25	AlMg1Si0.6 sB (5,1 GPa)/AlMg1Si10 (4,3 GPa)	AlMg1Si0.6 sB (8,5 MPa)/AlMg1Si10(7,3 MPa)	0,07/0,06
Tensile properties of composite metal foam and composite metal foam core sandwich panels [87]	Steel	2,9 and 3,1 g/cm^3	0,36 and 0,39	4,36-8,26 GPa	75–85 MPa (ss-cmf)/165 MPa (ss-cmf-cps)	0,02/0,04
DEFORMATION BEHAVIOUR OF CLOSED-CELL ALUMINIUMFOAMS IN TENSION [93]	Aluminium	0,25 g/cm^3 and 0,40g/cm^3	0,09 and 0,14	2360 MPa	4 MPa	0,03
Characterisation and simulation of tensile deformation of non-uniform cellular aluminium until damage [86]	Aluminium	0,5 g/cm^3	0,18	3.,5 GPa	5 MPa	0,05
The mechanical properties and modeling of a sintered hollow sphere steel foam [83]	Steel	–	0,15	3150 MPa	4.9 MPa	0,015
Fracture toughness of titanium foams for medical applications [96]	Titanium	0,3-0,4	0,06-0,08	116 GPa	61.1 MPa (r.density 0,4) and 56.4 MPa (r.density 0.3)	0,96
TOUGHNESS OF ALUMINIUM ALLOY FOAMS [92]	Aluminium	–	–	–	–	–
Combinatorial structural-analytical models for the prediction of the mechanical behaviour of isotropic porous pure metals [90]	Fe + NaCl/Ti + NaCl	–	0,43	–	–	–
Initial yield behaviour of closed-cell aluminium foams in biaxial loading [97]	Aluminium	–	0,117 & 0,172	1,07 GPa and 1,45 GPa	2 MPa and 3 MPa	0,015 & 0,021
Primary Investigation on an Iron Foam Sandwich Structure [89]	Iron	–	–	–	–	–
Investigation of the Behavior of Open Cell Aluminum Foam [98]	Aluminium	–	0,06-0,08	148- 452 MPa	1,32-2,08 MPa	2,14 x 10^{-3}-6,55 x 10^{-3}
Experimental investigation of mechanical properties of metallic hollow sphere structures [82]	Steel	0,3–0,6 g/cm^3	0,11-0,23	260-360 MPa	5,2 MPa	0,001-0,0017

make deductions for its behaviour.

In this work, we will outline our experimental work to reliably determine the Tensile Strength and Elastic Modulus of steel foam hollow sphere assemblies under the application of a tensile load and compare them with published data and scaling curves in order to evaluate the testing protocol used and determine the mechanical characterisation of steel foam hollow sphere assemblies under tensile load [84]. The present research aims to show reliable results for these two tensile characteristics and form the basis for future experimental investigations of similar structures, without employing expensive infrastructure such as DIC or X-ray tomographers [99,100]. The investigation will further investigate the validity and spectrum of application of the testing protocol by testing specimens of various relative densities, comprising spheres of two different sizes in different proportions. It aims to expand their use in industry, discuss differences observed between theoretical (design) and experimental values from previous research, and point out possible reasons for deviations.

2. Materials and preparation methods

The steel hollow spheres used in creating our test specimens are shown in Fig. 1, and their properties were provided by the manufacturer (Hollomet GmbH) as shown in Table 2. A thermosetting adhesive, Araldite AT1-1 (https://www.wellmid.com/down/down/Araldite AT1-1.pdf Huntsman/Vantico, 2000), was used to pre-coat the spheres. Thermosetting adhesives like Araldite AT1-1 are one-component adhesives that require an elevated temperature to activate and cure. Once cured, the adhesive can reach a lap shear strength of 32–33 MPa and drum peel strength of 4–6 MPa. The spheres comprise FeCuP alloy, with carbon levels reaching 0.14 % and 0.17 % for the two types (sizes) of spheres available. Spheres labelled “SHS2” had an average diameter of 2.3 mm, while “SHS4” had an average diameter of 4.5 mm. The selection of sphere diameters was based on the manufacturer’s availability, and the same batch was used for Yiatros et al. [1]. For continuity, we use the same terminology as Yiatros et al. [1], referring to specimens with 2 mm diameter spheres as SHS2 and 4 mm diameter spheres as SHS4.

Fig. 1. Pre-coated steel foam hollow spheres are used for specimen creation.

Furthermore, the actual shell walls of the sphere have pores; hence, steel foam spheres SHS2 had 10 % microporosity, and SHS4 had 12 % [1]—Fig. 2A and 2B show microscope measurements of the sphere’s diameters. Surface morphology was studied using scanning electron microscopy (SEM) using a FEI Quanta 200 microscope (Hillsboro, OR, USA) with an acceleration voltage of 20 kV and a working distance of 10 mm. Before SEM analysis, the specimens underwent sputter-coating with gold to ensure proper conductivity and prevent charging effects during imaging.

Table 2
Physical properties of steel hollow spheres [1].

Sphere Type	C-Content(%)	Average diameter D (mm)	Apparent Density (g/cm^3)	Shell wall thickness t (μm)	Micro-Porosity (%)	Adhesive mass (%)	$t/_R$
SHS2	0,14	2,3	0,5	43–53	10	15	0,04
SHS4	0,17	4,5	0.4	64–74	12	13	0,03

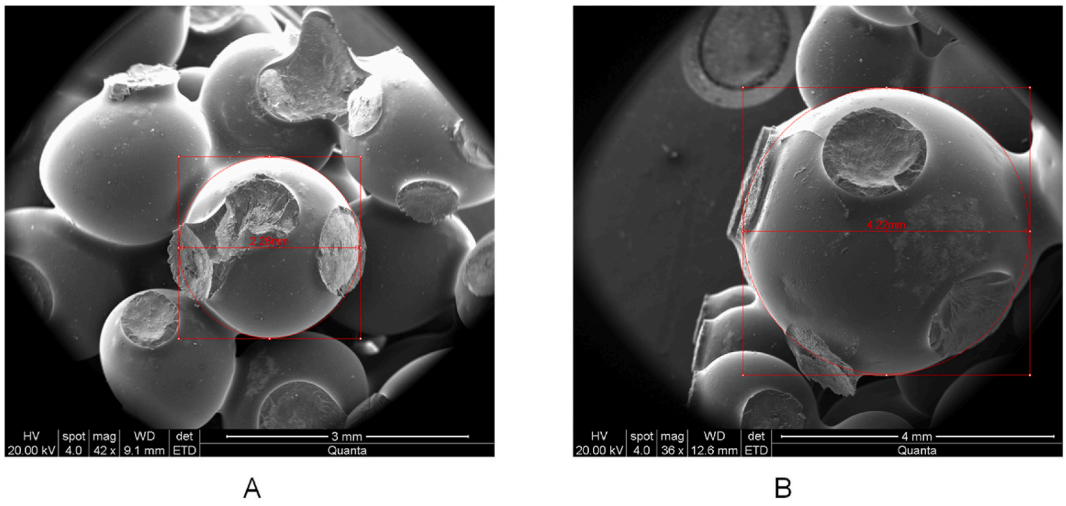

Fig. 2. Measurement of sphere diameter by the microscope, A) SHS2, B) SHS4.

The specimen geometry was guided by the shape of the flatwise grip (50 mm × 50 mm cross-sectional area), and it was decided to keep the height approximately the same, drawing from a similar attribute for the compression tests undertaken in Yiatros et al [1]. 50 mm ensures that there will be at least 10 cells in any given axis for the specimens in question. Although a more elaborate geometry (i.e. dogbone coupons) as seen in other works [83], could have been considered in an attempt to focus failure in the middle third of the specimen, it was deemed appropriate to try out the new grips testing protocol with a more uniform geometry and assess the need for a more elaborate geometry at a

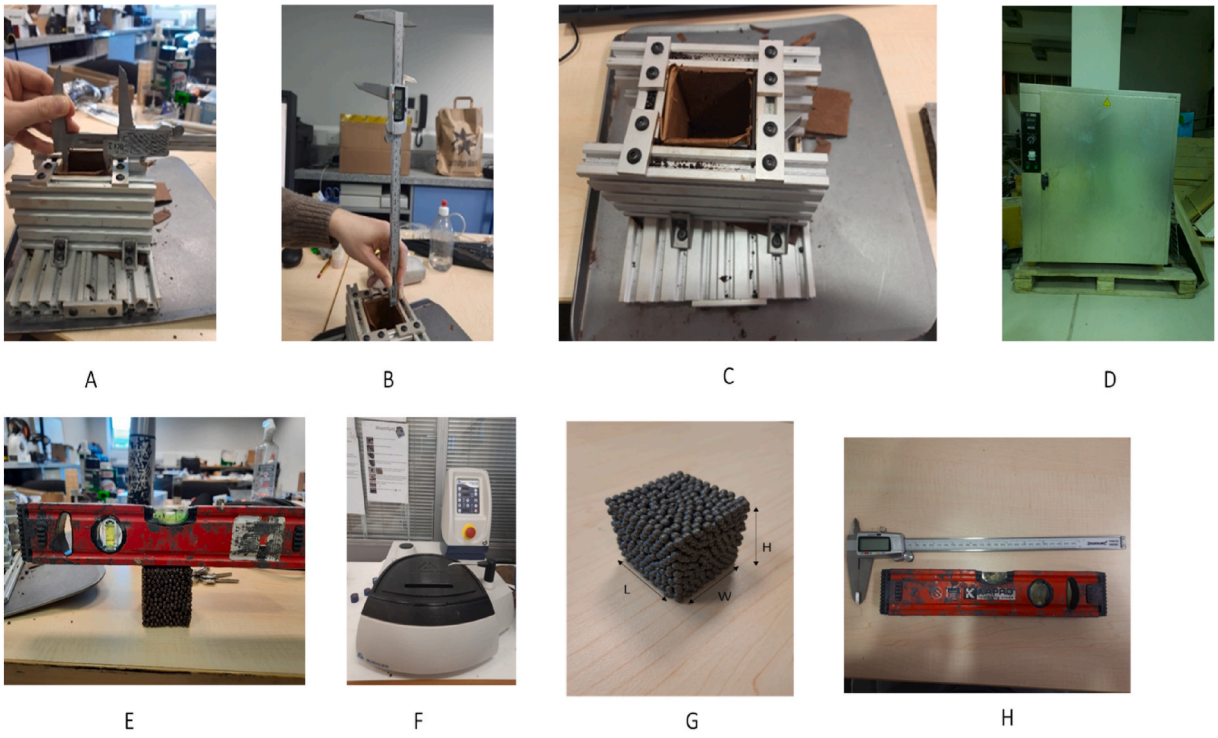

Fig. 3. A) Setting distance between the mould walls B) Measurement of the depth of the mould C) Bespoke mould for prototypes of 50 × 50 × 50 mm^3 steel hollow spheres specimens D) Industrial oven where the mould enters to become the connection of the spheres between them through the heat and final specimen construction E) Levelling of specimen surfaces F) Vertical head sanding machine for specimens preparation prior to the tests G) The dimensions to be measured H) The tools used to measure the specimens' dimensions and level surfaces.

later stage.

The specimen preparation process can be summarised in the following stages/steps.

1. Preparation of mould at the correct size (Fig. 3A).
2. Measurement of the height of the mould empty area where the spheres will be placed (Fig. 3B).
3. The specimens are made using steel hollow spheres placed in a bespoke mould (Fig. 3C). Inserting the spheres into the mould at a height corresponding to the final height of the specimen. Add a metal plate to achieve the desired height and apply pressure to the surface.
4. Measurement of final dimensions before placing the mould in the industrial oven.
5. Placement of mould in an industrial oven (Fig. 3D) in the laboratory for 2 h at 200 °C for adequate activation and curing of the thermo-setting adhesive. Keeping the temperature and time of curing fixed, assuming the same volume of araldite AT1-1 coating on the spheres, was implemented as an assurance for observing the same curing conditions and avoiding deviations in the quality of the bonds.
6. When the specimen comes out of the industrial oven, it is checked for flatness on the side that will connect to the grips (Fig. 3E). If not, sand it on the vertical head sanding machine (Fig. 3F).
7. The specimen dimensions are measured (Fig. 3G) and then joined to the grips using epoxy adhesive. Fig. 3H presents the tools used to measure the specimens.

It has to be noted here that only minor out-of flatness cases were treated in point 6 of the preparation workflow as high out-of-flatness specimens were rejected. In any case, the treated surface was fully submerged in the binding adhesive connecting to the grips, making any potential microcracks introduced into the specimen irrelevant.

All tests took place at the Large Structures Laboratory at Cyprus University of Technology, Department of Civil Engineering and Geomatics, using the Lloyds 150 kN Universal Testing System shown in Fig. 4.

A vernier calliper and a spirit level were used to measure the specimens. The vernier calliper was selected because it ensures higher accuracy in the measurements taken in the aforementioned specimen preparation steps. Since the width and length of the specimens were constrained by the mould, the height was the only variable in the prototyping process. Pre-curing the height was allowed to be about 52 mm, and a mild pressure was applied to the grips holding the top and bottom plates to ensure that the top and bottom surfaces were flat, while the expected marginal shrinkage due to curing would not create any voids within the specimen. This limit was chosen after various tests on the heights of the sphere assemblies during step 3 of the aforementioned specimen preparation methodology. All height measurements were made as shown in Fig. 3B from the top edge to the base of the mould. As the results presented below demonstrate, acceptable deviations from the required dimensions post-curing should be between ± 2 to 3 mm from the required dimensions for a specimen to be acceptable for testing. At this point, it should be emphasised that continuous measurements of the dimensions of the specimen from the same sides are recommended. For this, it is helpful to place identification marks at the location of each side of the specimen according to its position in the mould during step 6.

A commercial epoxy (J-B Weld) was used to bond the specimens to the tensile grip tabs. In contrast to other epoxies, J-B Weld is a superior adhesive, much stronger (ultimate tensile strength above 35 MPa) and stiffer than the specimen's typical strength and stiffness, successfully concentrating tensile failure within the specimen depth rather than the interface with grip tabs. Before initiating the test, an optical specimen check is performed before placing it in the test frame. During this check, any imperfections on the specimen or the connection between the specimen and the grip tabs are recorded. After that, the specimen with tabs is placed in the test frame and fixed with a pivot rod, which allows in plane rotation. For this test series, special grips for flatwise tension were used (Fig. 5), which are also used to test flat tensile strength and tensile adhesion properties according to several standards for other materials (ASTM C297 [101], ASTM D3354 [102], ASTM D1623BASTM D1623 − 17 [103], EN 1607[104], EN 2243-4[105]). The experimental parameters are set through the corresponding console software that connects to the test frame. Upon specimen placement, displacement and load are set to zero. The whole experiment was done under displacement control with a displacement rate of 30 mm/hr (0.5 mm/min), which is the accepted displacement rate for similar flatwise tensile tests according to ASTM C297(ASTM-C297, 2010). After the experiments, the grips

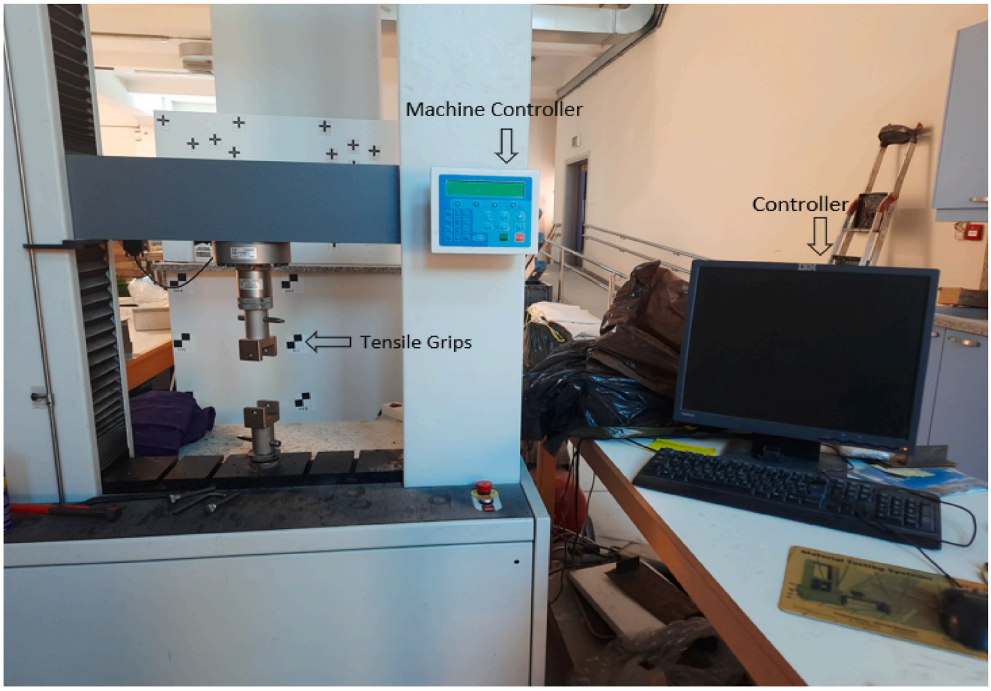

Fig. 4. The Lloyds 150 kN testing machine is set for a tensile test.

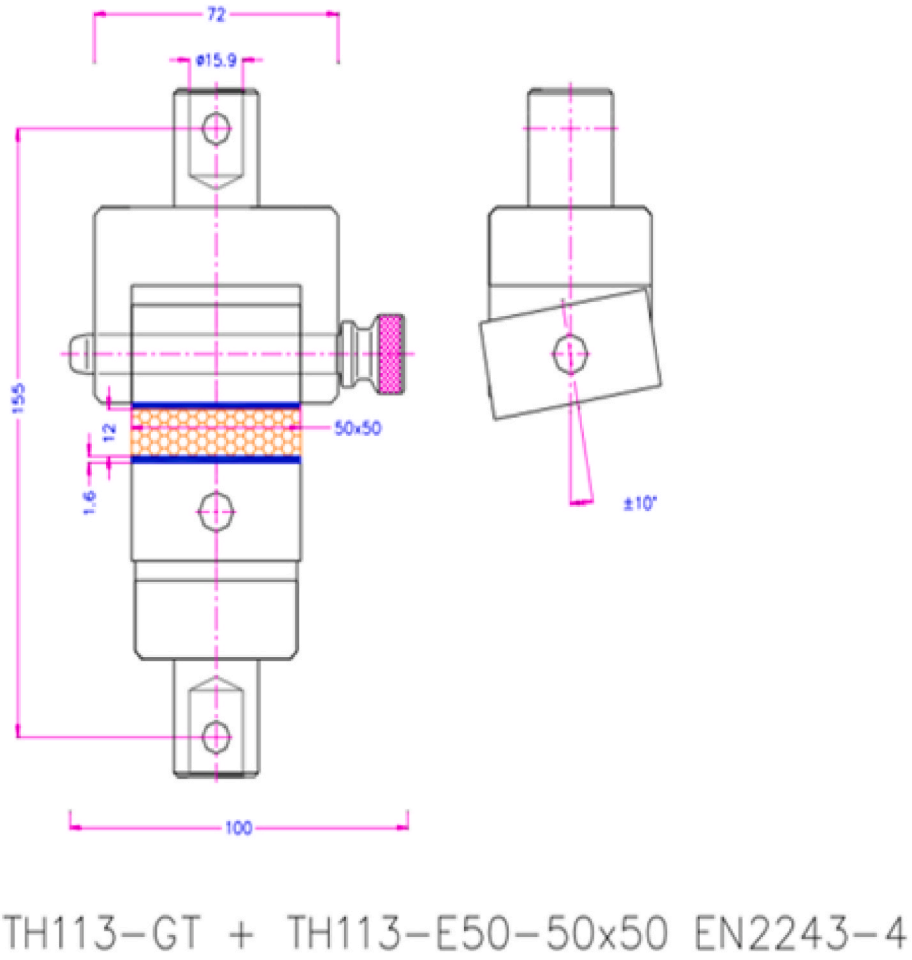

Fig. 5. Tensile strength test fixtures. Produced by Grip-Engineering Thümler GmbH.

were cleaned of isolated epoxy using a vertical head sanding machine. First, a check is made for the crack point, and if it coincides with the initial points that were located. Some of the steps mentioned above are presented in Fig. 6.

The specimen's shape is a cube with dimensions 50 × 50 × 50 mm^3. The first series of experiments was performed with specimens made with solely 2 mm sphere assemblies (SHS2) and 4 mm sphere assemblies (SHS4), aiming for specimens with two distinct average relative densities. The reported type of specimens differed only in relative density. Hence, the first series of experiments has two groups of specimens. A subsequent investigation using mixtures of the two types of spheres in different proportions was also performed to generate intermediate average densities, presented in the subsequent sections. More specifically, in the second series of experiments, specimens were prepared with a mixture of the two available sphere diameters. Three different groups of specimens were prepared; "SHS2_0,75_SHS4_0,25″ comprising 75 % by volume of 2 mm spheres (and 25 % by volume 4 mm spheres), "SHS2_0,50_SHS4_0,50″ comprising a 50 %:50 % ratio of 2 mm and 4 mm spheres, and finally "SHS2_0,25_SHS4_0,75″ comprising 25 % by volume 2 mm spheres (and 75 % by volume 4 mm spheres).

For completeness, in Table 3, one can observe the specimen groups and the number of specimens in each group.

3. Results

3.1. Physical and mechanical properties of specimens

Table 4 shows the physical characteristics of the specimens with 2 mm sphere assemblies. Numbering in brackets indicates specimen number. The specimen numbers omitted refer to mostly imperfect specimens (specimens with initially cracked sections or imperfect surfaces) or, in fewer instances, specimens where the test failure occurred at the interface with the grips due to imperfect adhesion.

Table 5 shows the physical characteristics of the specimens with 4 mm sphere assemblies.

The volume of the specimens is found by measuring each side at three locations and weighing each specimen on a laboratory balance. The physical characteristics of the specimens in each set are closely distributed about two distinct mean density values, 0,585 g/cm^3 for SHS2 specimens and 0,469 g/cm^3 for SHS4, respectively, with minimal standard deviations as the respective coefficients of variation indicate.

Tables 6–7 presents testing specimens' Elastic modulus and Tensile strength. The value of Elastic's Modulus corresponds to the initial or second (where available) elastic slope of the curve of the stress-strain diagram for each specimen [106]. The values of tensile strength are derived from: $\sigma_{max} = F_{max}/A$, where F_{max} is the maximum (peak) load, and A is the original cross-sectional area [107]. The relative density of the specimens is benchmarked on $\rho_{s,}$ which is taken as the density of solid steel (ρ_s = 7.87 g/cm^3) [108]. The relative density term is the typical packing density quantification expression, indicative of the size of the porosity and typical for metal foams for comparison purposes.

Figs. 7 and 8 show the stress-strain curves from specimen tests. The strain is presented in percentage form to make it easier to compare the results with previous works, since most authors have chosen this form of presentation of the results concerning the strain. It is presented as a percentage of the original height of the specimen.

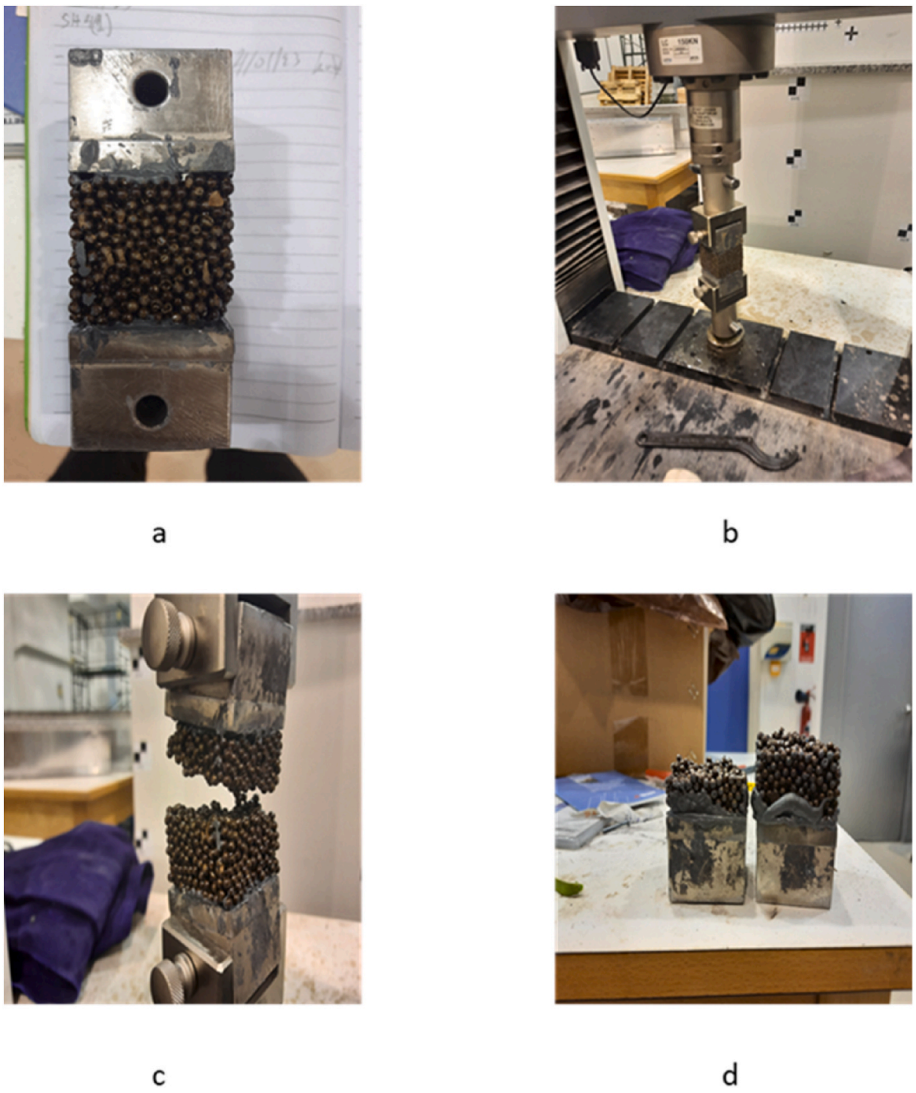

Fig. 6. a) Optical check of the specimen before the experiment, b) Specimen placed in the machine, c) Specimen just after the end of the experiment, d) Optical check of the specimen after the experiment.

Table 3
Number of specimens per group.

Specimen	Number of specimens
SHS2	12
SHS4	9
SHS2_0,75_SHS4_0,25	6
SHS2_0,5_SHS4_0,5	5
SHS2_0,25_SHS4_0,75	5

All specimens exhibited similar stress-strain behaviour, with limited deviations and an initial "toe" of varying strain attributed to the tab alignment, followed by a linear increase and a brittle failure at peak load. As seen in Figs. 7 and 8, the testing procedure for some specimens (SHS2(7), SHS2(12), SHS(19)-SHS2(21), SHS4(7), SHS4(9), SHS4(10), SHS4(16)) included a loading-unloading-reloading scenario. This load loop was executed in a sample of the specimens in an attempt to verify the elasticity of the quasi-linear path of the specimens under question and investigate the similarity of the stiffness magnitude compared to the monotonically loaded specimens. The loading-unloading-reloading limits were selected to be well below (>70 %) of a conservative tensile strength value that was observed in early trials. Specifically for specimens of 50 × 50 × 50 mm^3, we used a limit of 4.5 kN loading for

Table 4
The physical characteristics of the specimens with 2 mm sphere assemblies. Where L is the length of the specimen, W is the width of the specimen, and H is the height of the specimen.

No	Specimen	Mass (g)	L (mm)	W (mm)	H (mm)	Density (g/cm^3)
1	SHS2(4)	79	53,082	53,417	49,290	0,565
2	SHS2(5)	77	50,603	56,093	47,505	0,571
3	SHS2(6)	74	51,802	50,523	50,783	0,557
4	SHS2(7)	73	51,598	49,372	49,798	0,575
6	SHS2(12)	71	49,988	50,125	49,190	0,576
7	SHS2(14)	71	47,913	50,497	51,527	0,570
8	SHS2(17)	76	48,442	51,985	52,083	0,579
9	SHS2(18)	81	51,373	52,045	51,095	0,593
10	SHS2(19)	78	48,555	52,287	48,570	0,633
11	SHS2(20)	71	51,800	48,982	45,565	0,614
12	SHS2(21)	80	50,535	52,322	50,718	0,597
	Mean	**75,55**	**50,517**	**51,604**	**49,648**	**0,585**
	Standard Dev.	**3,58**	**1567**	**1935**	**1828**	**0,022**
	Coefficient of Variation (%)	**4,74**	**3,10**	**3,75**	**3,68**	**3,76**

Table 5
The physical characteristics of the specimens with 4 mm sphere assemblies. Where L is the length of the specimen, W is the width of the specimen, and H is the height of the specimen.

No	Specimen	Mass (g)	L (mm)	W (mm)	H (mm)	Density (g/cm^3)
1	SHS4(1)	59	47,385	52,155	51,857	0,460
2	SHS4(3)	54	51,265	44,120	51,623	0,462
3	SHS4(7)	55	50,882	50,477	44,428	0,482
4	SHS4(9)	59	51,175	50,197	51,512	0,446
5	SHS4(10)	54	49,050	48,670	50,133	0,451
6	SHS4(13)	60	47,507	51,787	51,203	0,476
7	SHS4(14)	62	49,727	52,253	50,093	0,476
8	SHS4(15)	59	47,688	51,795	47,603	0,502
9	SHS4(16)	62	51,807	49,702	52,115	0,462
	Mean	**58,22**	**49,609**	**50,128**	**50,063**	**0,469**
	Standard Dev.	**2,97**	**1668**	**2419**	**2382**	**0,016**
	Coefficient of Variation (%)	**5,10**	**3,36**	**4,83**	**4,76**	**3,41**

SHS2 and 2.5 kN for SHS4, before unloading to 1.5 kN and reloading to failure. 4.5 kN and 2.5 kN were selected as much lower than the failure load of the first monotonically loaded SHS2 and SHS4 specimens, respectively. The loading-unloading-reloading protocol was only used for some specimens, as the reloading slopes did not exhibit major deviations from the monotonically loaded specimens.

Although both sets of specimens had uniform relative densities, their mechanical properties exhibited mild variation in the results. This is expected as the tensile stiffness and strength of the specimens depend on the number, direction, and quality of bonds holding each assembly together. Recording these two mechanical properties for the two test specimen groups, it can be observed that the Elastic Moduli ranged between 273,92 and 430,12 MPa with a mean of 340,89 MPa for SHS4 and 325,51 to 470,33 MPa with a mean of 399,28 MPa for SHS2, exhibiting the expected behaviour of smaller cells and higher density, leading to more a stiffer response. Furthermore, for the tensile strength the SHS4 specimens were ranging from 1,93 to 4,46 MPa with a mean of 2,8 MPa, while for SHS2, the range was 2,36 to 4,36 MPa with a mean 3,53 MPa. The mechanical properties results for each specimen group indicate low to moderate coefficients of variation, a characteristic of quasi-uniform foams. This may not be typical for metal foams, but the use of metal foam spheres leading to a better control of the pore distribution can attribute to this.

Regarding the location (plane) of failure (Fig. 11), the most significant proportion of SHS4 specimens exhibited failure in the middle third of the specimen height, while almost all SHS2 specimens would fail near the top or bottom third, but always within the specimens, as failures on or including the interface were not included. Furthermore, close examination of the failure planes indicates that the failure is driven by the rupture of bonds rather than hollow sphere ruptures. This is proven by Figs. 9 and 10, taken from the microscope. In these Figures, sphere separation marks are visible on the epoxy surface where the detached sphere left its shape. The results are tabulated in Table 8.

The specimens presented in Table 8 were produced in two different occasions. Specimens SHS2(4–14) and SHS4(1–13) were initially produced and sanded before joining onto the grip tabs. The second batch was prepared with higher dimensional precision not to require sanding before joining the grip tabs. This exploratory exercise was undertaken in order to explore the effect of sanding on the specimens and whether it would have an impact on the position of the plane of failure (i.e., the

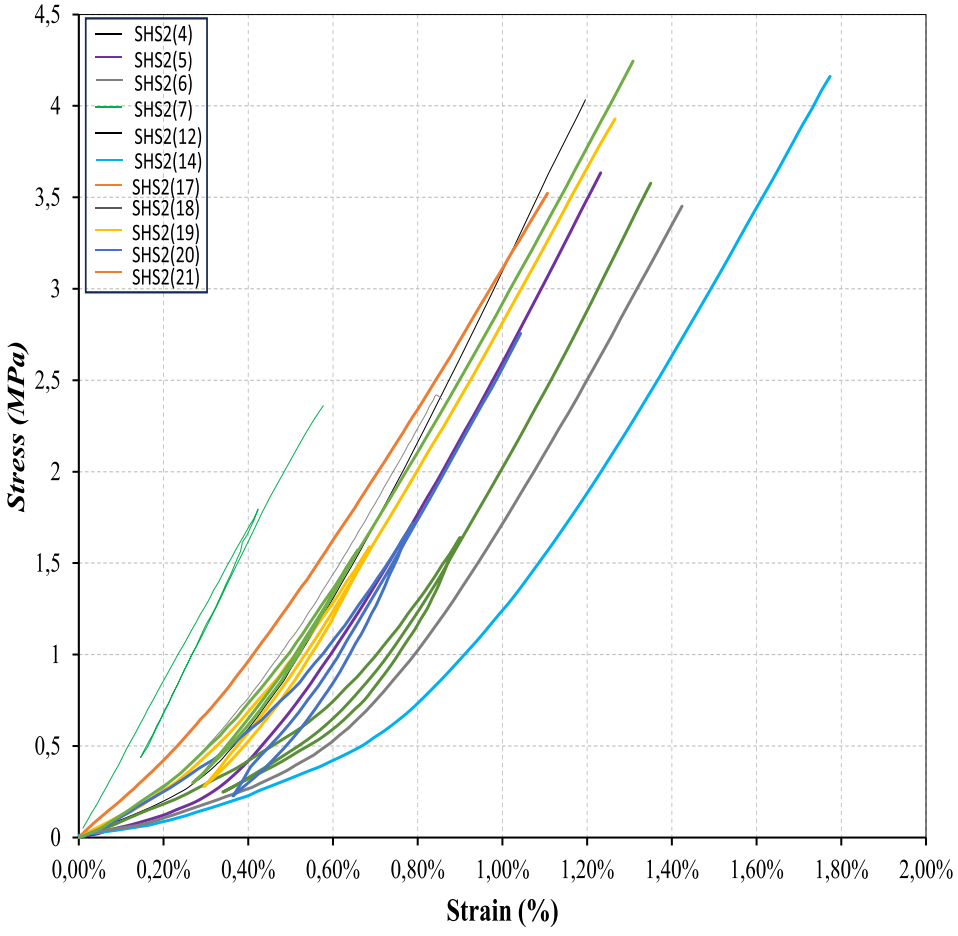

Fig. 7. The stress-strain curves of each specimen of the experimental group of SHS2 specimens.

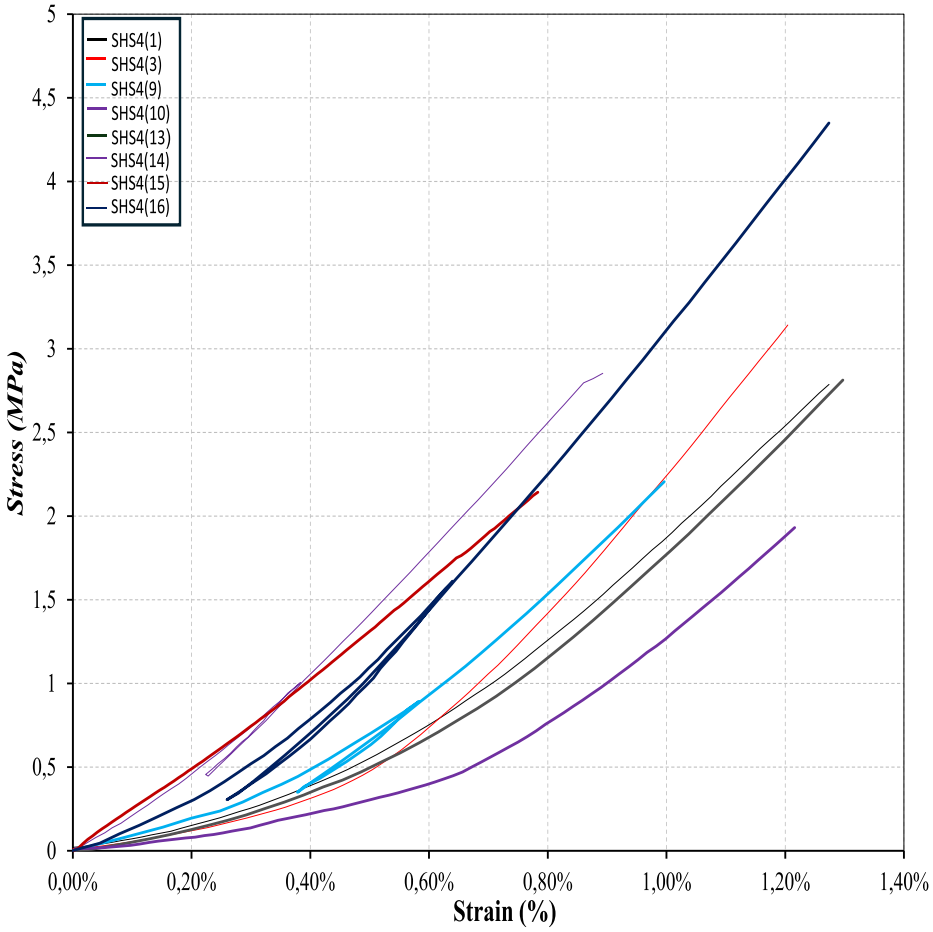

Fig. 8. The stress-strain curves of each specimen of the experimental group of SHS4 specimens.

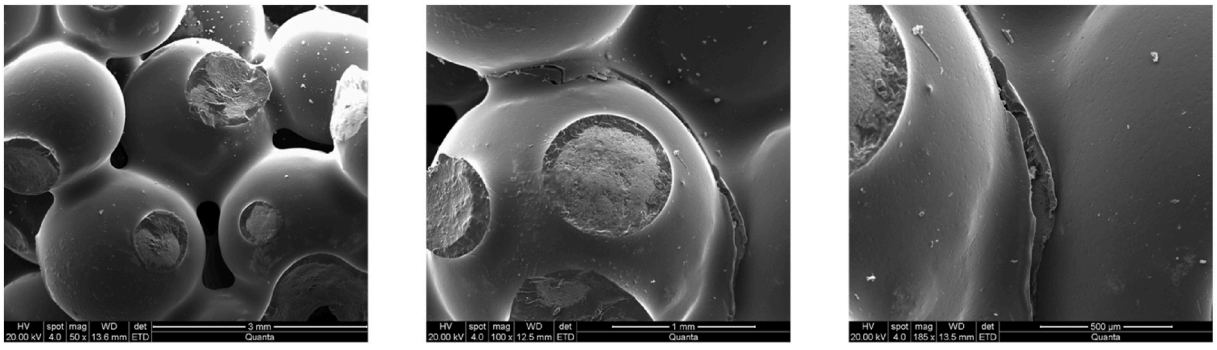

Fig. 9. Determination of the crack surface for the specimen with 2 mm spheres by the microscope.

onset of micro-cracks near the surface), but as the results in Table 7 indicate, there was no notable deviation from the previous results.

3.2. Specimen preparation process for mixed sphere assembly specimens

Building on the promising results from the first specimen groups and the viability of the testing protocol, the next investigation focused on the suitability of the protocol for specimens with different relative densities. Given the availability of metal foam spheres of two sizes, we decided to explore the possibility of relative density as a design parameter and how it affects the mechanical properties (Elastic modulus and Tensile strength) by combining the two types of spheres in different proportions. Mixing aggregates of different sizes in different proportions can give rise to improved results due to the increased number and geometric complexity of bonds formed and the improvement of packing (see Fig. 12) in such assemblies at a lower relative density compared to the relative density of SHS2.

In this investigation, three types of specimen groups (assemblies) were produced, where the proportion of 2 mm spheres was 25 %, 50 %, 75 %, and 4 mm spheres was 75 %, 50 %, 25 % by volume, respectively; their production process is as follows.

- First, the requested spheres are placed in a measuring glass, where 50 ml corresponds to 25 % of the total specimen.
- After the requested quantity has been measured, the spheres are transferred to another container where the mixture is made.

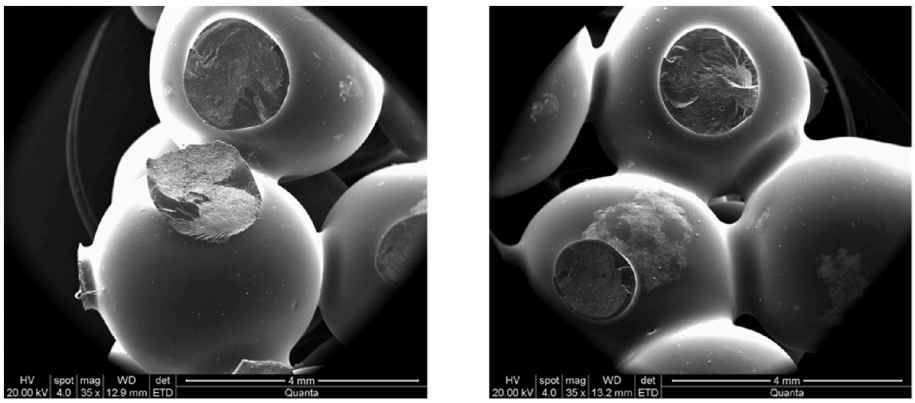

Fig. 10. Determination of the crack surface for the specimen with 4 mm spheres by the microscope.

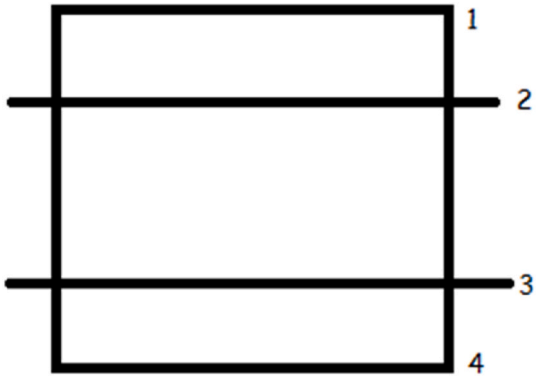

Fig. 11. The zones of the specimen.

Table 6
The Elastic modulus and Tensile strength of testing specimens with 2 mm sphere assemblies (SHS2).

No	Specimen	Elastic modulus, E (MPa)	Tensile strength, σ_{max} (MPa)	Relative density (ρ/ρ_s)
1	SHS2(4)	435,34	4,03	0,0716
2	SHS2(5)	419,35	3,70	0,0723
3	SHS2(6)	376,07	2,42	0,0705
4	SHS2(7)	470,33	2,36	0,0728
5	SHS2(12)	417,79	3,75	0,0729
6	SHS2((14)	392,28	4,16	0,0721
7	SHS2(17)	325,51	3,52	0,0733
8	SHS2(18)	388,14	3,45	0,0751
9	SHS2(19)	389,40	4,07	0,0801
10	SHS2(20)	374,43	3,00	0,0777
11	SHS2(21)	403,44	4,36	0,0755
	Mean	**399,28**	**3,53**	**0,0740**
	Standard Dev.	**35,65**	**0,65**	**0,0027**
	Coefficient of variation (%)	**8,92**	**18,4**	**3,65**

- Then, the procedure described above is repeated for the specimens with a single sphere type. The mixed specimens were made by volume measurement because it was assumed to be a safer method for achieving the same size as the one type of sphere specimen. Fig. 13 shows the mixing process.
- The labelling of the mixed assemblies was SHS2_XX_SHS4_YY, where XX and YY would be the percentage proportions of each constituent sphere type, and the summation of the percentage proportions should always be 100 %. Fig. 14 shows all the types of specimens used in the current research, with their labels in the caption.

Table 7
The Elastic modulus and tensile strength of testing specimens with 4 mm sphere assemblies (SHS4).

No	Specimen	Elastic modulus, E (MPa)	Tensile strength, σ_{max} (MPa)	Relative density (ρ/ρ_s)
1	SHS4(1)	317,55	2,79	0,058
2	SHS4(3)	430,12	3,14	0,059
3	SHS4(7)	378,74	2,74	0,061
4	SHS4(9)	305,45	2,27	0,056
5	SHS4(10)	372,31	2,85	0,057
6	SHS4(13)	308,74	2,88	0,060
7	SHS4(14)	273,92	1,93	0,060
8	SHS4(15)	275,70	2,14	0,064
9	SHS4(16)	405,50	4,46	0,058
	Mean	**340,89**	**2,80**	**0,059**
	Standard Dev.	**53,88**	**0,70**	**0,002**
	Coefficient of Variation	**15,81**	**25,00**	**3,39**

Table 8
The zone where the crack started per specimen.

Specimen	Zone 1–2 or 3-4	Zone 2-3
SHS2(4)	X	
SHS2(5)	X	
SHS2(6)	X	
SHS2(7)	X	
SHS2(12)	X	
SHS2(14)	X	
SHS2(17)	X	
SHS2(18)		X
SHS2(19)	X	
SHS2(20)		X
SHS2(21)	X	
SHS4(1)		X
SHS4(3)	X	
SHS4(7)		X
SHS4(9)		X
SHS4(10)	X	
SHS4(13)		X
SHS4(14)	X	
SHS4(15)	X	
SHS4(16)	X	

3.3. Physical and mechanical properties of mix specimens

Table 9 shows the physical characteristics of the specimens with 2 and 4 mm spheres.

It is evident from the very low coefficients of variation on the bulk density (under 5 %) for all specimen groups, as well as for the rest of the geometric properties, despite the rudimentary and manual character of

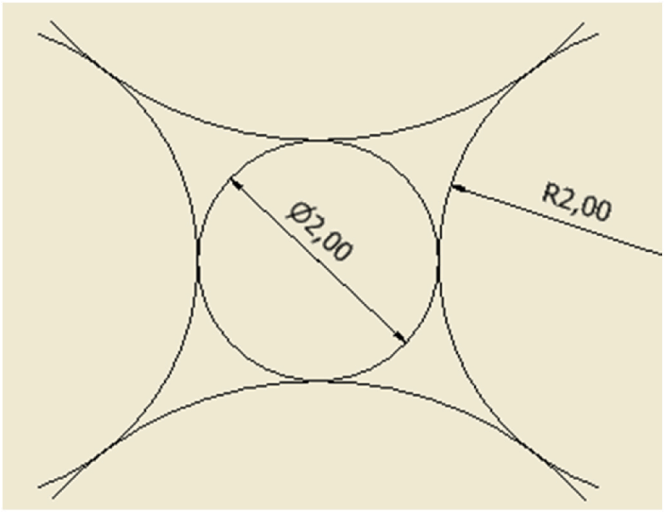

Fig. 12. The ideal combination of spheres of two different sizes, minimising inter-sphere voids.

the specimen preparation process. The tests followed the same procedure as in the previous section, and Tables 10–12 present the mechanical properties (Elastic Modulus and Tensile Strength) for each specimen.

The results for each relative density group exhibited very good and, in some cases, excellent correlation. Especially on the elastic modulus, a low coefficient of variation is observed, while the coefficient of variation is moderate for the tensile strength was in a moderate range.

Figs. 15–17 shows the stress-strain curves from specimen tests. The strain is presented in percentage form to make it easier to compare the results with previous works, since most authors have chosen this form of presentation of the results concerning the strain. It is presented as a percentage of the original height of the specimen.

The stress-strain paths of the mixed sphere assemblies indicate differing trends for the different mixture proportions. For instance, it is clear that with more than 50 % of SHS2 spheres in the mix, the average tensile elastic modulus can be very close to the mean Elastic modulus of the SHS2 assemblies. Furthermore, it is also evident that the presence of 25 % SHS2 spheres in the mixture can push the mean tensile strength close to the mean tensile strength for SHS2, while for the SHS2_0,75_SHS4_0,25 specimens, the mean tensile strength was superior to the equivalent mean of SHS2 assemblies. It should also be noted that while for most groups, the standard deviations for both Elastic modulus and tensile strength were consistent with the earlier sets of experiments, the SHS2_0,75_SHS4_0,25 exhibited an even lesser coefficient of variation in comparison with the other groups. From Fig. 18, we can highlight that the small amount of 2 mm spheres leads to a significant improvement in the strain a specimen can take before cracking compared with the specimens with only 4 mm spheres (Fig. 8).

Table 13 summarises the location where the plane of failure is found. It is evident here that the plane of failure is now located in zone 2 for the vast number of specimens. This can be attributed to the preparation process, in which, during placement, there might be some higher concentration of smaller (SHS2) spheres near the ends rather than the middle, making the relative density across the depth of the specimen moderately graded towards the top and bottom. The presence of larger (SHS4) spheres in the middle offers fewer bonds and, thus, a more attractive position for the failure to be initiated and propagated. As it became visible in some images from the microscope, the smaller spheres take positions between the larger ones (see Fig. 18). Also, as in the case of specimens with one type of sphere, the separation between the spheres is due to a crack in the epoxy. Fig. 19 shows the start of the crack between 2 spheres.

3.4. Elastic modulus and tensile strength variability

Fig. 20 shows the relationship between elastic modulus and relative density for all tested specimens across the five groups. Each data point represents an individual specimen, and symbols are used to distinguish the different configurations (SHS2, SHS4, and their mixtures). The results demonstrate a clear positive correlation between relative density and elastic modulus, consistent with theoretical models for cellular materials. Specimens belonging to the SHS4 group, which exhibited the lowest relative density, clustered in the lower modulus range (≈280–350 MPa). In contrast, SHS2 specimens, with the highest relative density, achieved elastic moduli in excess of 400 MPa, with several specimens approaching 480 MPa. The hybrid groups occupied intermediate positions: SHS2_0.25_SHS4_0.75 and SHS2_0.5_SHS4_0.5 displayed moderate stiffness, while SHS2_0.75_SHS4_0.25 approached the performance of SHS2, indicating the beneficial effect of higher SHS2 sphere content. Although some scatter is evident, particularly within SHS2 and SHS2_0.5_SHS4_0.5, the overall distribution of low to moderately low coefficients of variation for each specimen group

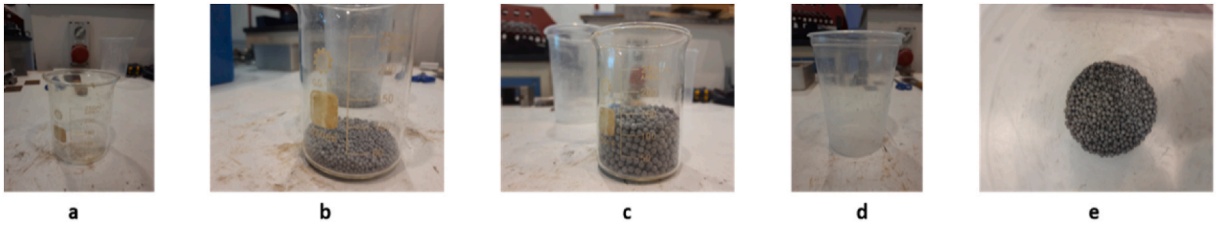

Fig. 13. a) Empty beaker b) 2 mm sphere quantities for SHS2_0,25_SHS4_0,75 specimen c) 4 mm sphere quantities for SHS2_0,25_SHS4_0,75 specimen d) Beaker for the mix of spheres e) final mixture.

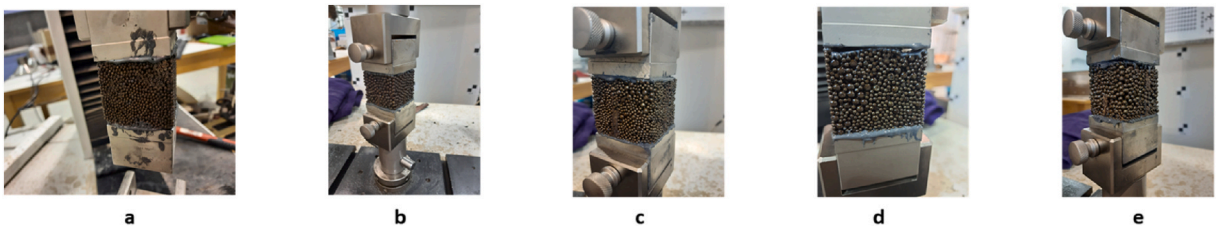

Fig. 14. a) SHS2 b) SHS4 c) SHS2_0,75_SHS4_0,25 d) SHS2_0,5_SHS4_0,5 e) SHS2_0,25_SHS4_0,75.

Table 9
The physical characteristics of the specimens with 2 and 4 mm spheres. Where L is the length of the specimen, W is the width of the specimen, and H is the height of the specimen.

No	Specimen	Mass (g)	L(mm)	W (mm)	H (mm)	Density (g/cm^3)
1	SHS2_0,75_SHS4_0,25(1)	74	49,547	49,758	49,612	0,605
2	SHS2_0,75_SHS4_0,25(2)	73	48,505	50,998	50,615	0,583
3	SHS2_0,75_SHS4_0,25(3)	73	47,902	51,372	51,132	0,580
4	SHS2_0,75_SHS4_0,25(5)	73	47,343	53,178	52,453	0,553
5	SHS2_0,75_SHS4_0,25(6)	73	48,123	52,290	52,228	0,555
6	SHS2_0,75_SHS4_0,25(10)	75	49,762	51,997	52,025	0,557
	Mean	**73,5**	**48,530**	**51,599**	**51,344**	**0,572**
	Standard Dev.	**0,76**	**0,868**	**1075**	**1004**	**0,019**
	Coefficient of Variation (%)	**1,03**	**1,80**	**2,10**	**1,96**	**3,32**
No	Specimen	Mass (g)	L(mm)	W(*mm*)	H (mm)	Density (g/cm^3)
1	SHS2_0,5_SHS4_0,5(1)	66	51,653	51,745	47,770	0,517
2	SHS2_0,5_SHS4_0,5(3)	73	47,882	52,123	52,060	0,580
3	SHS2_0,5_SHS4_0,5(5)	63	47,312	50,758	50,835	0,516
4	SHS2_0,5_SHS4_0,5(6)	70	48,910	52,160	51,953	0,528
5	SHS2_0,5_SHS4_0,5(8)	70	48,778	52,272	52,013	0,528
	Mean	**68,40**	**48,907**	**51,812**	**50,926**	**0,534**
	Standard Dev.	**3,50**	**1494**	**0,556**	**1643**	**0,024**
	Coefficient of Variation (%)	**5,12**	**3,05**	**1,07**	**3,22**	**4,49**
No	Specimen	Mass (g)	L(mm)	W (mm)	H (mm)	Density (g/cm^3)
1	SHS2_0,25_SHS4_0,75(1)	68	50,125	51,680	51,230	0,512
2	SHS2_0,25_SHS4_0,75(2)	71	51,435	50,972	51,235	0,529
3	SHS2_0,25_SHS4_0,75(3)	71	47,730	52,217	51,665	0,551
4	SHS2_0,25_SHS4_0,75(4)	66	49,433	49,673	51,770	0,519
5	SHS2_0,25_SHS4_0,75(9)	66	48,338	52,507	52,073	0,499
	Mean	**68,40**	**49,412**	**51,410**	**51,595**	**0,522**
	Standard Dev.	**2,24**	**1310**	**1013**	**0,325**	**0,018**
	Coefficient of Variation (%)	**3,27**	**2,65**	**1,97**	**0,63**	**3,45**

Table 10
The elastic modulus and tensile strength of testing specimens with mixing spheres.

No	Specimen	Elastic Modulus, E (MPa)	Tensile Strength, σ_{max} (MPa)	Relative Density (ρ/ρ_s)
1	SHS2_0,75_SHS4_0,25 (1)	379,52	3,99	0,077
2	SHS2_0,75_SHS4_0,25 (2)	405,67	4,04	0,074
3	SHS2_0,75_SHS4_0,25 (3)	409,41	4,57	0,073
4	SHS2_0,75_SHS4_0,25 (5)	337,90	3,79	0,070
5	SHS2_0,75_SHS4_0,25 (6)	385,33	4,46	0,070
6	SHS2_0,75_SHS4_0,25 (10)	406,69	4,21	0,071
	Mean	**387,42**	**4,17**	**0,072**
	Standard Dev.	**24,86**	**0,27**	**0,002**
	Coefficient of variation (%)	**6,42**	**6,47**	**2,78**

Table 11
The elastic modulus and tensile strength of testing specimens with mixing spheres.

No	Specimen	Elastic Modulus, E (MPa)	Tensile Strength, σ_{max} (MPa)	Relative Density (ρ/ρ_s)
1	SHS2_0,50_SHS4_0,50 (1)	456,05	4,86	0,0654
2	SHS2_0,50_SHS4_0,50 (3)	367,50	3,43	0,0701
3	SHS2_0,50_SHS4_0,50 (5)	362,88	3,14	0,0653
4	SHS2_0,50_SHS4_0,50 (6)	352,66	2,72	0,0669
5	SHS2_0,50_SHS4_0,50 (8)	378,82	3,22	0,0668
	Mean	**383,58**	**3,47**	**0,0669**
	Standard Dev.	**37,19**	**0,73**	**0,0017**
	Coefficient of Variation (%)	**9,70**	**21,0**	**2,54**

Table 12
The elastic modulus and tensile strength of testing specimens with mixing spheres.

No	Specimen	Elastic Modulus E (MPa)	Tensile Strength, σ_{max} (MPa)	Relative Density (ρ/ρ_s)
1	SHS2_0,25_SH4_0,75(1)	379,06	3,99	0,065
2	SHS2_0,25_SH4_0,75(2)	388,60	3,75	0,067
3	SHS2_0,25_SH4_0,753)	354,62	3,76	0,070
4	SHS2_0,25_SH4_0,75(4)	295,74	2,49	0,066
5	SHS2_0,25_SH4_0,75(9)	306,18	3,35	0,063
	Mean	**344,84**	**3,47**	**0,066**
	Standard Dev.	**37,65**	**0,53**	**0,002**
	Coefficient of Variation (%)	**10,9**	**15,3**	**3,03**

confirms the strong influence of relative density on stiffness.

Similarly, Fig. 21 presents the tensile strength of individual specimens as a function of relative density for the five aforementioned configurations. The data points reveal a general upward trend, indicating that tensile strength increases with relative density, which is in line with expectations for cellular and composite structures. The SHS4 specimens, which correspond to the lowest relative densities, consistently exhibited the weakest performance, with tensile strengths clustered around 2.0–3.0 MPa. By contrast, SHS2 specimens, with the highest relative densities (≈0.074–0.075), reached strengths in excess of 4.5 MPa, with several specimens approaching 5.0 MPa. Similarly to the elastic modulus diagram the hybrid groups occupied intermediate positions: SHS2_0.25_SHS4_0.75 and SHS2_0.5_SHS4_0.5 produced moderate strengths with noticeable scatter (moderate coefficients of variation), whereas SHS2_0.75_SHS4_0.25 exhibited strengths close to those of SHS2, demonstrating the beneficial effect of a higher SHS2 fraction.

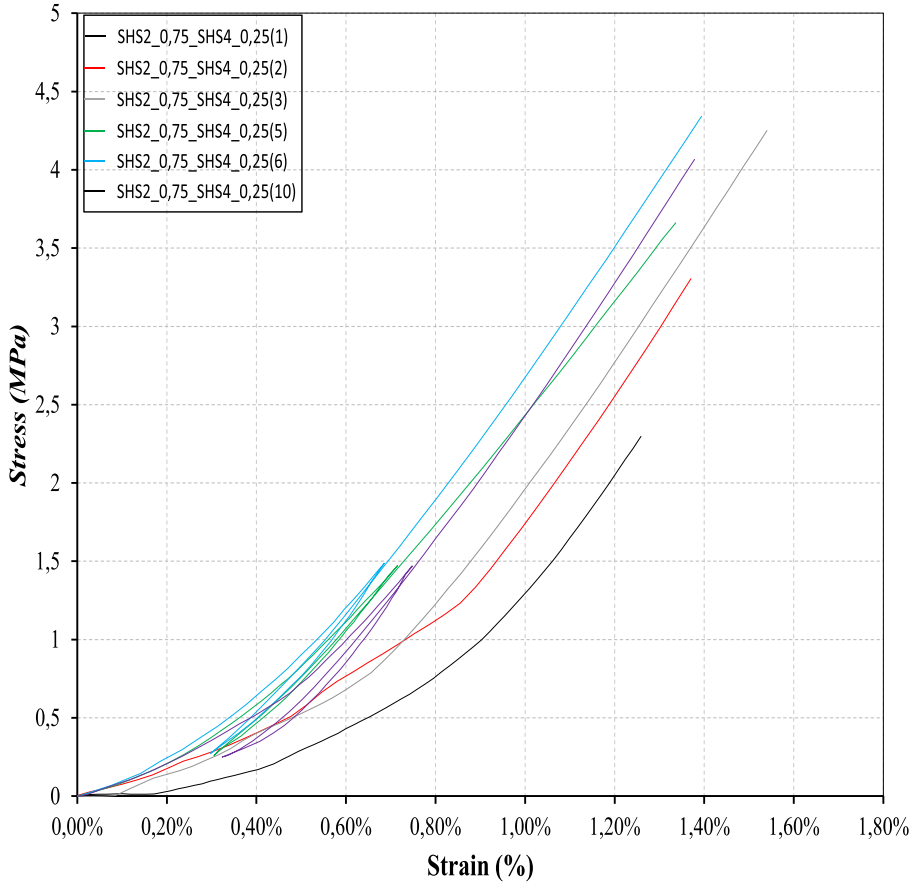

Fig. 15. The stress-strain curves of each specimen of the experimental group of SHS2_0,75_SHS4_0,25 specimens.

The mechanical response of the specimens showed a clear dependence on both relative density and material configuration. Fig. 22 illustrates the elastic modulus results in a box and whiskers plot, where stiffness increased systematically with relative density. The SHS4 group exhibited the lowest median modulus (~310 MPa) and the highest coefficient of variation, while the SHS2 group achieved the maximum stiffness (>400 MPa). Hybrid configurations provided intermediate performance, with SHS2_0.75_SHS4_0.25 combining high modulus with the lowest coefficient of variation, suggesting a beneficial balance between stiffness and reliability. A one-way ANOVA confirmed significant differences among groups (**$p < 0.05$**), and post-hoc analysis indicated that SHS4 was significantly weaker than SHS2 and the higher-density hybrids.

A similar trend was observed for tensile strength (Fig. 23). SHS4 again exhibited the lowest values (median ~2.5 MPa), whereas the highest strengths (>4.0 MPa) were recorded for SHS2 and SHS2_0.75_SHS4_0.25. The hybrid groups displayed intermediate properties, with SHS2_0.25_SHS4_0.75 showing moderate strength and low scatter, and SHS2_0.5_SHS4_0.5 showing greater variability. Statistical analysis confirmed significant group differences (**$p < 0.05$**), with post-hoc tests revealing SHS4 as significantly weaker than all other configurations.

These results are consistent with the Gibson–Ashby models for cellular materials, which predict the elastic modulus and strength scale with relative density according to power-law relationships. The observed increase in both modulus and tensile strength with relative density aligns with these theoretical design expectations. Moreover, the performance of the hybrid groups suggests that compositional tailoring can improve not only stiffness and strength but also reduce scatter of the mechanical properties results in this type of testing, which is particularly important given the inherent variability in cellular structures[95]. Overall, the results establish a consistent positive correlation between relative density and mechanical performance. While SHS2 provides the highest stiffness and strength, hybrid configurations—particularly SHS2_0.75_SHS4_0.25—achieve comparable performance with improved reproducibility, indicating that carefully balanced mixtures can optimize both strength and reliability.

Fig. 24 shows data relative to the Elastic modulus of foams, E/E_s , plotted against relative density, ρ/ρ_s. The solid lines represent the scaling equations found in Gibson and Ashby [84]. The solid blue curve represents the scaling curve for open-cell foam. The solid orange and grey curves represent the scaling curves for closed-cell foam with $\varphi = 0.8$ and $\varphi = 0.6$, respectively. These are described by the following equations:

$$E \Big/ E_s = \varphi^2(\rho/\rho_s)^2 + (1-\varphi)(\rho/\rho_s),$$

where $\varphi = 1$ for open-cell foam and $\varphi = 0.6$ or $\varphi = 0.8$ for closed-cell foam, φ is the volume fraction of the solid contained at the edges of the cells, and the remaining fraction (1-φ) is the face. Fig. 25 shows data for Relative Tensile Strength, σ_{max}/σ_{ys} , plotted against relative density, ρ/ρ_s, The solid blue, orange, and grey curves represent the analogous equations for open cell, close cell, and hollow sphere metal foam, respectively. The following equations describe the above curves:

$$\sigma_{max} \Big/ \sigma_{ys} = 0.3(\rho/\rho_s)^{1.5} \text{ (open cell)},$$

$$\sigma_{max} \Big/ \sigma_{ys} = 0.33(\rho/\rho_s)^2 + 0.44(\rho/\rho_s) \text{ (close cell)},$$

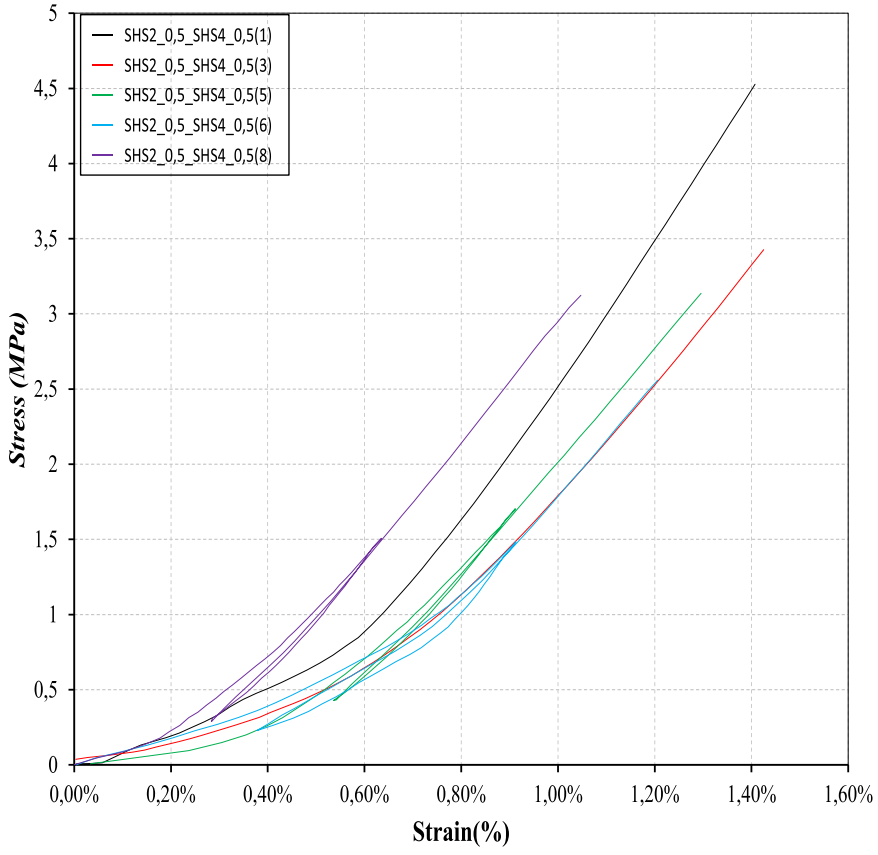

Fig. 16. The stress-strain curves of each specimen of the experimental group of SHS2_0,5_SHS4_0,5 specimens.

$\sigma_{max} \Big/ \sigma_{ys} = 0.65(\rho/\rho_s)^{1.36}$(hollow sphere) [112].

The individual points are distinct values for past works that have also been presented in Ref. [95], and the results obtained in the present work, as average values for each set, are presented in Figs. 24 and 25.

As can be seen from Figs. 24–25, the results obtained from the experiments fit quite well with the values from the scaling equations on a log scale, compared to other published data of similar tests from the literature. This promising comparison can be attributed to the proposed testing protocol as a suitable and inexpensive method to test metal foams and metal sphere assemblies.

3.5. Number of bonds

To better understand the specimens' microstructure, we study the number of grains per type of specimen. Grain analysis was done using Gwyddion [109]. Gwyddion is a multiplatform, modular free software for visualisation and analysis of data from scanning probe microscopy (SPM) techniques. The method used is Grains – Mark by Threshold, which detects bonds based on colour. The number of bonds in Table 14 is the average of five specimens.

As expected, the specimens with 2 mm had more significant bonds. The reduction of the 2 mm spheres reduces the number of expected bonds. When the ratio of 4 mm spheres increases, this negatively impacts the number of bonds. A significant difference is observed between the specimens having greater than or equal to 50 % 2 mm spheres regarding the number of bonds developed. At this point, it should be emphasised that the test was done on the crack point, which is the point with the smallest number of bonds between the spheres. An essential role in the structure and position of the spheres is also played by the mix performed during the manufacture of the specimens and the randomness concerning the spheres' position within the specimen. The number of bonds is shown in Table 14.

The contact surface of the spheres is not constant, as shown in Fig. 26, which is to be expected due to the random position of each sphere within the mould used to make the final specimens.

3.6. Statistical analysis of the standard deviation of the mechanical properties of the specimens

In this section, the standard deviation of the mechanical properties (Elastic Modulus and Tensile Strength) are evaluated regarding the reliability of the standard deviation values in terms of statistical confidence. The Standard Deviation and Confidence Interval data for Standard Deviation were obtained and presented in Table 15 for Elastic's Modulus and Table 16 for Tensile Strength.

All results are within the confidence interval based on the results obtained and combined with those presented in Tables 1, 6 and 7–12.

Also, to strengthen the result, ANOVA (Analysis of Variance) was performed. For the Elastic Modulus and Tensile Strength, the p-value is 0.04 and 0.02, respectively. The generally acceptable limits for ANOVA are $p < 0.05$ [110], which indicates that the means for the properties of the groups are statistically different. Table 17 shows the results of ANOVA for Elastic Modulus, and Table 18 shows the results for Tensile Strength.

Post-hoc analysis (Tukey HSD) was also performed to determine which groups differed significantly. Tukey's Honestly Significant Difference (HSD) is a post-hoc test used after a significant Analysis of Variance (ANOVA) to determine which specific pairs of group means are statistically different from each other [111]. The post-hoc analysis results showed that no statistical differences were observed in the case of

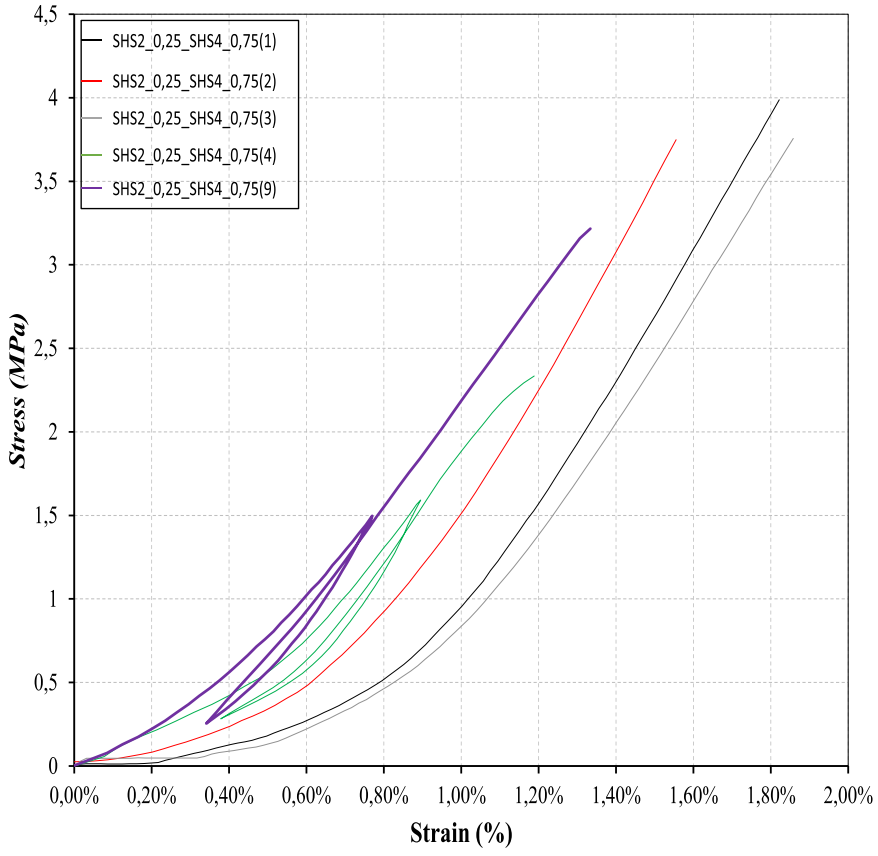

Fig. 17. The stress-strain curves of each specimen of the experimental group of SHS2_0,25_SHS4_0,75 specimens.

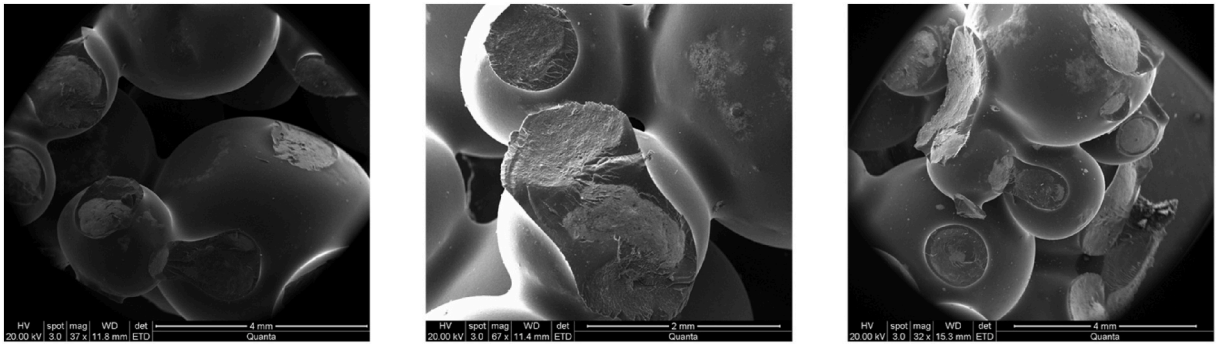

Fig. 18. Microscope figure of the connection between spheres of different sizes.

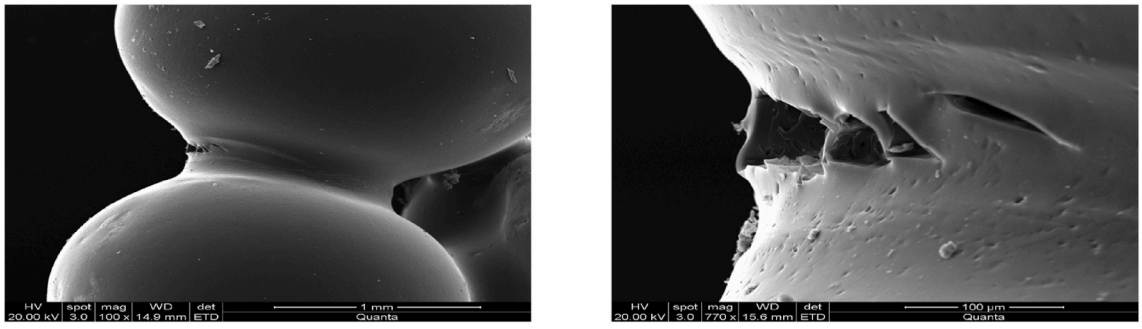

Fig. 19. Microscope figure of the start of the crack between 2 spheres.

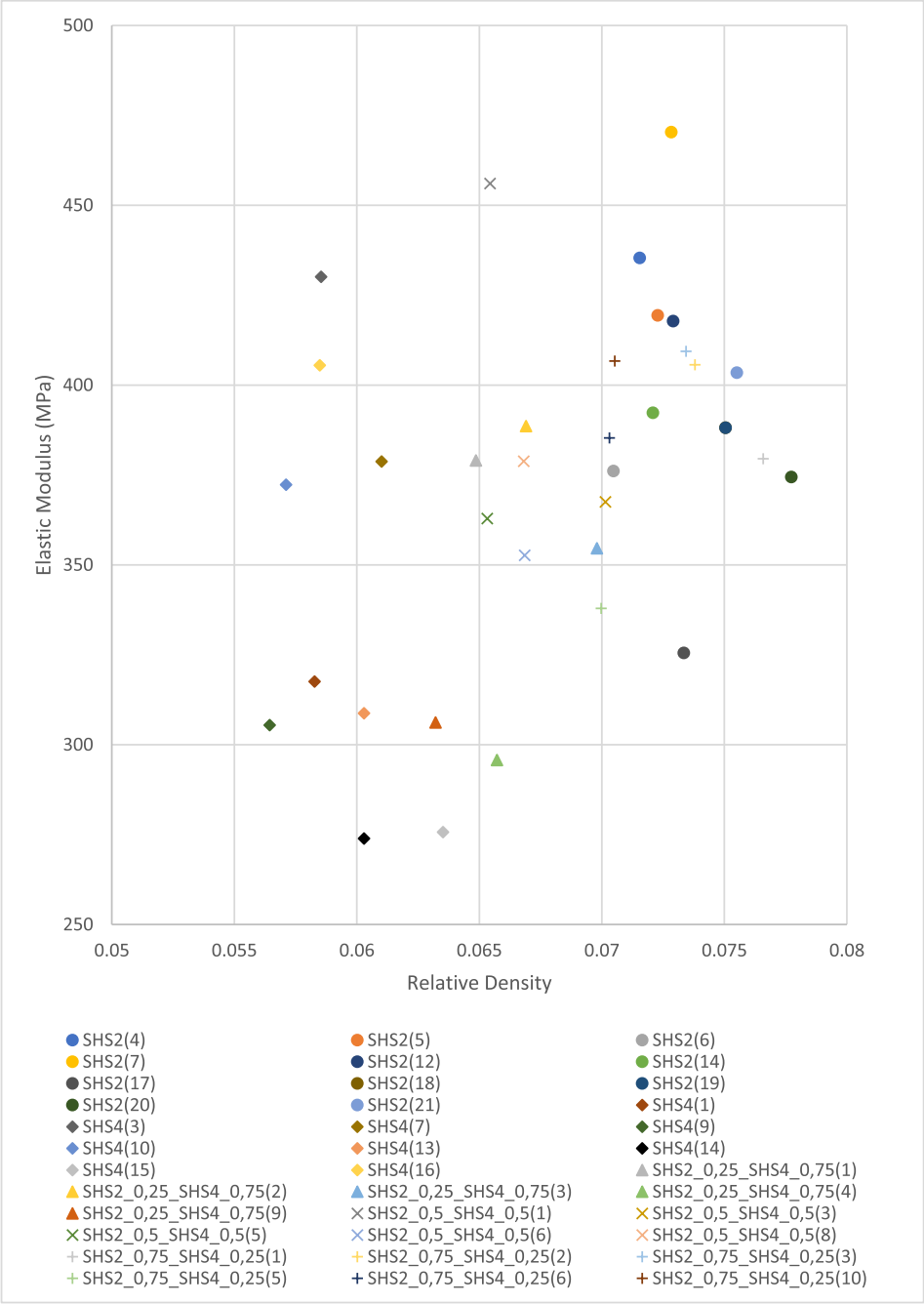

Fig. 20. Values obtained from the current work for Elastic Modulus against Relative Density. Circles indicate the SHS2 specimens, rhombuses indicate the SHS4 specimens, triangles indicate the SHS2_0,25_SHS4_0,75 specimens, x indicate the SHS2_0,50_SHS4_0,50 specimens, and crosses indicate the SHS2_0,75_SHS4_0,25 specimens.

the Elastic Modulus. Statistical differences were observed in Tensile Strength only between SHS4(G2) and SHS2_0,75_SHS4_0,25(G3). The post-hoc analysis results are presented in Tables 19 and 20 for Elastic Modulus and Tensile Strength, respectively.

3.7. Discussion

The series of experiments using spheres of 2 diameters, either in single size specimens or hybrid specimens, has enabled the investigation of the tensile strength and elastic modulus for a range of relative densities. The mixture preparation method followed in the current research has led, in some instances, to a somewhat uneven distribution of spheres within specimens. More specifically, the proportion of spheres of the same size on the surface of the same type of specimens was different. The smaller spheres usually ended at the bottom of the mixture cup during the mix. Because mixing was done individually for each specimen, a concentration of the smaller diameter spheres was observed at the bottom of the mixing cup and at specific points in the specimens, possibly playing a role in the place where the cracks start. This could be explained by the number of bonds found at the points where the specimens broke, especially in the specimens with 75 % 4 mm spheres, which had almost the same number of bonds as those made up only of 4 mm spheres. A possible solution is to repeat mixing of spheres after the transfer to the mould.

To ensure consistency in specimen preparation, all specimens were manufactured following the same steps in sphere mixing, mould filling,

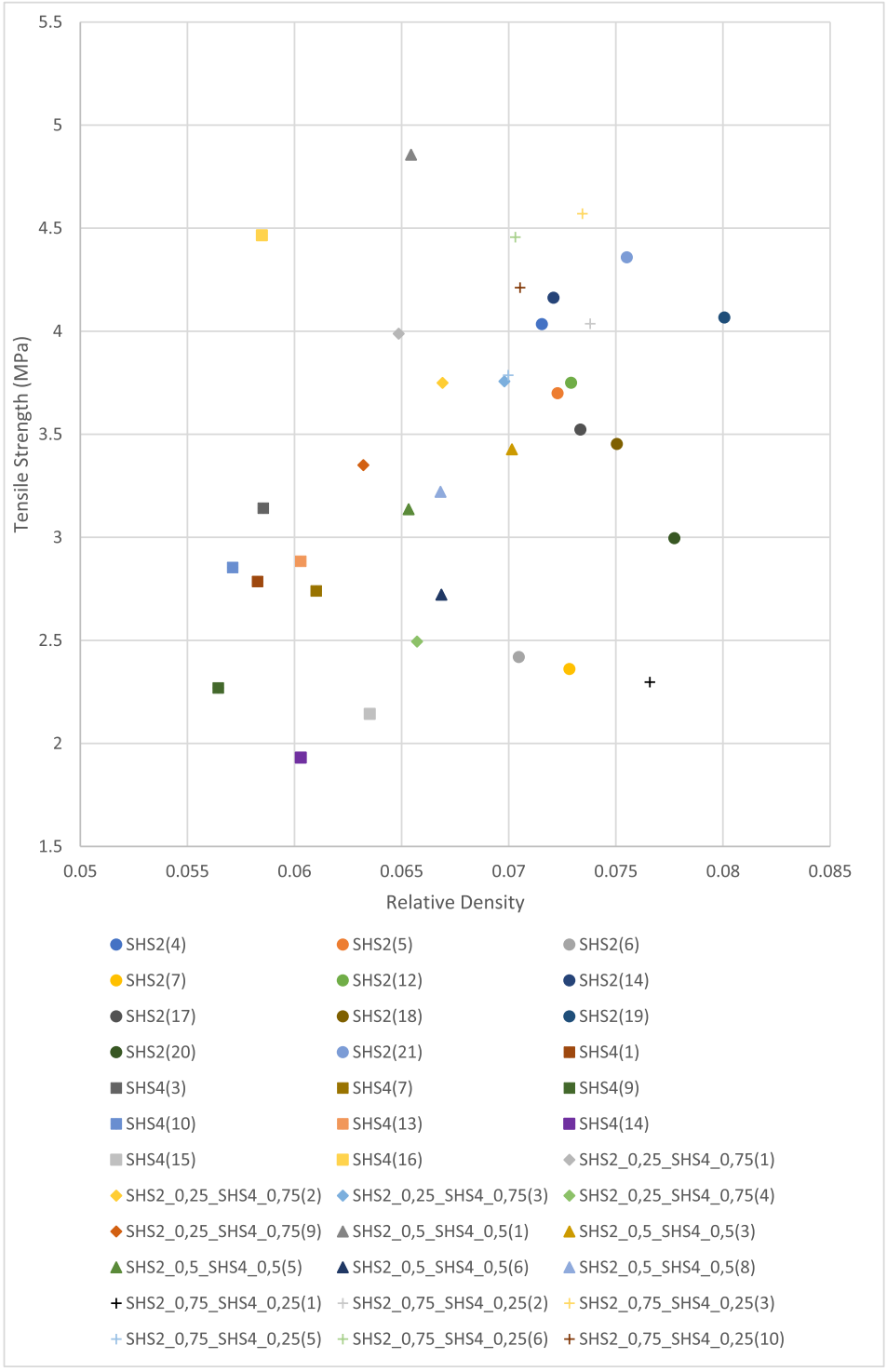

Fig. 21. Values obtained from the current work for Tensile Strength against Relative Density. Circles indicate the SHS2 specimens, squares indicate the SHS4 specimens, rhombuses indicate the SHS2_0,25_SHS4_0,75 specimens, triangles indicate the SHS2_0,50_SHS4_0,50 specimens, and crosses indicate the SHS2_0,75_SHS4_0,25 specimens.

the measurements during sample preparation, and the use of the same equipment. Also, as presented above, a statistical test was performed on the specimens' physical properties to ensure uniformity. Specimens that showed significant deviation either geometrically or visible fractures were rejected.

One more thing that can be highlighted is the crack position across the depth of the specimen. A few possible factors might have influenced crack initiation in the specimens. The treatment of specimens to mitigate for out of straightness at the top and bottom surfaces could play a role in initiating microcracks near these surfaces, but this is unlikely due to the use of the bonding adhesive to the grips, which could counteract such effects. Another factor could be the proportion of voids due to the random packing, where a concentration of cavities in a particular section of the specimen can create a weak zone for crack initiation. Finally, for the specimens with two different types of spheres, the contact bond of the different spheres can play a significant role in crack start

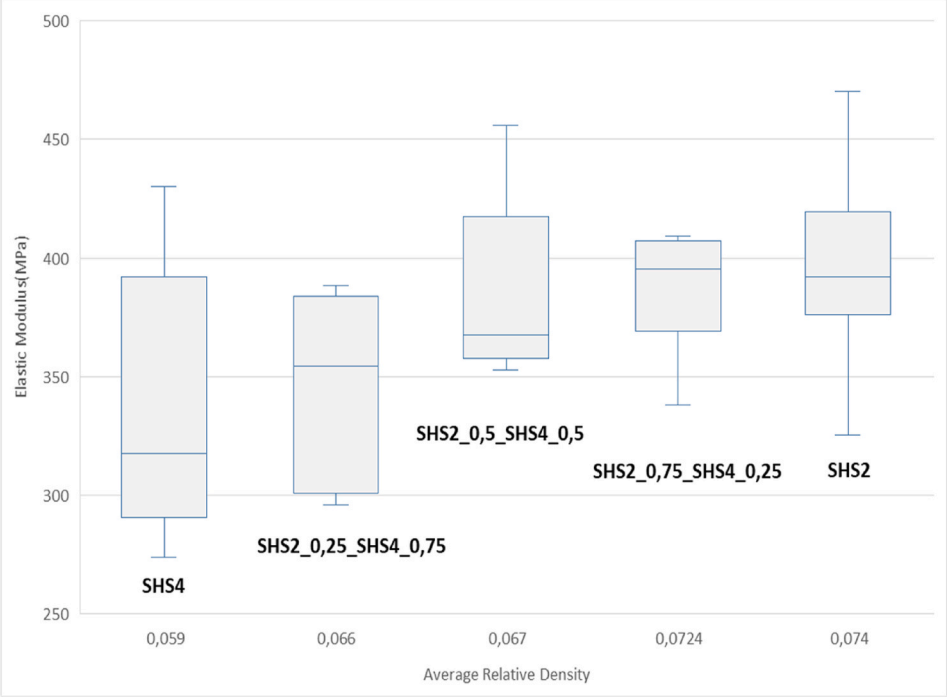

Fig. 22. The variability of Elastic's Modulus values per group of specimens. The number of specimens per group is: SHS2 is 12, SHS4 is 9, SHS2_0,75_SHS4_0,25 is 6, SHS2_0,5_SHS4_0,5 is 5, SHS2_0,25_SHS4_0,75 is 5.

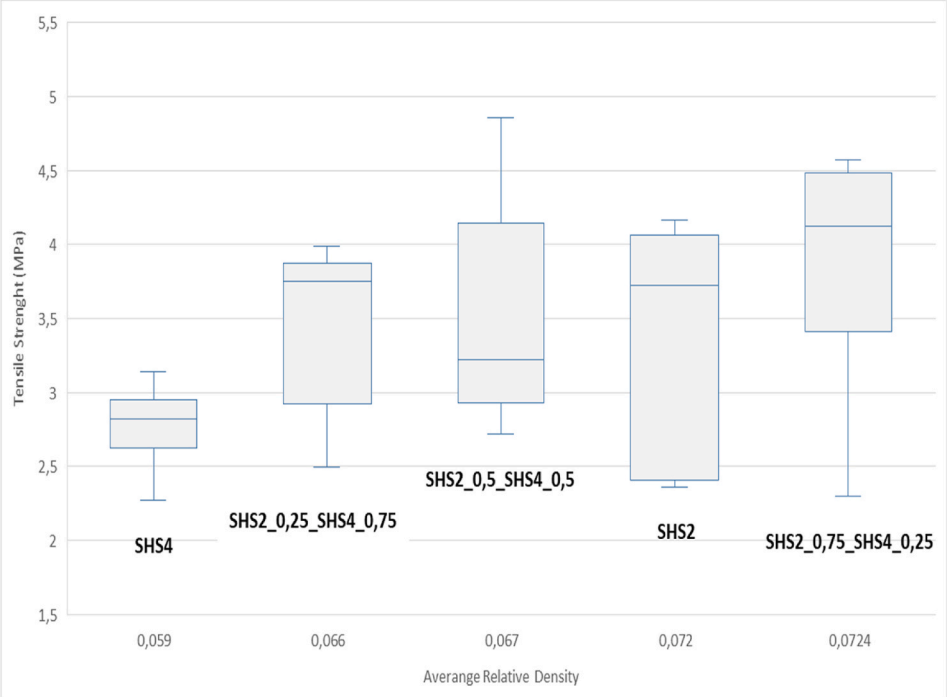

Fig. 23. The variability of Tensile Strength values per group of specimens. The number of specimens per group is: SHS2 is 12, SHS4 is 9,SHS2_0,75_SHS4_0,25 is 6, SHS2_0,5_SHS4_0,5 is 5, SHS2_0,25_SHS4_0,75 is 5.

initiation, again creating comparatively weaker zones within the specimen. As mentioned above, further experiments were carried out where specimens with only one sphere type were made. The results did confirm that the effect of the grinding of the specimens was unlikely to support crack initiation, strengthening the conviction for the other two possible factors affecting the location where cracks appeared, such as the points of connection between the spheres and possible cavities that appeared inside the specimens. At this point, it is worth highlighting that the cracks were exclusively related to sphere joint dislocations. Something that has also been observed in previous research [82,83].

According to Table 13, the mixing between the two types of spheres, regardless of the mixing ratios, indicates an improved transfer of stress through specimens, which is confirmed by the proportion of specimens exhibiting, on average, higher tensile stiffness and strength

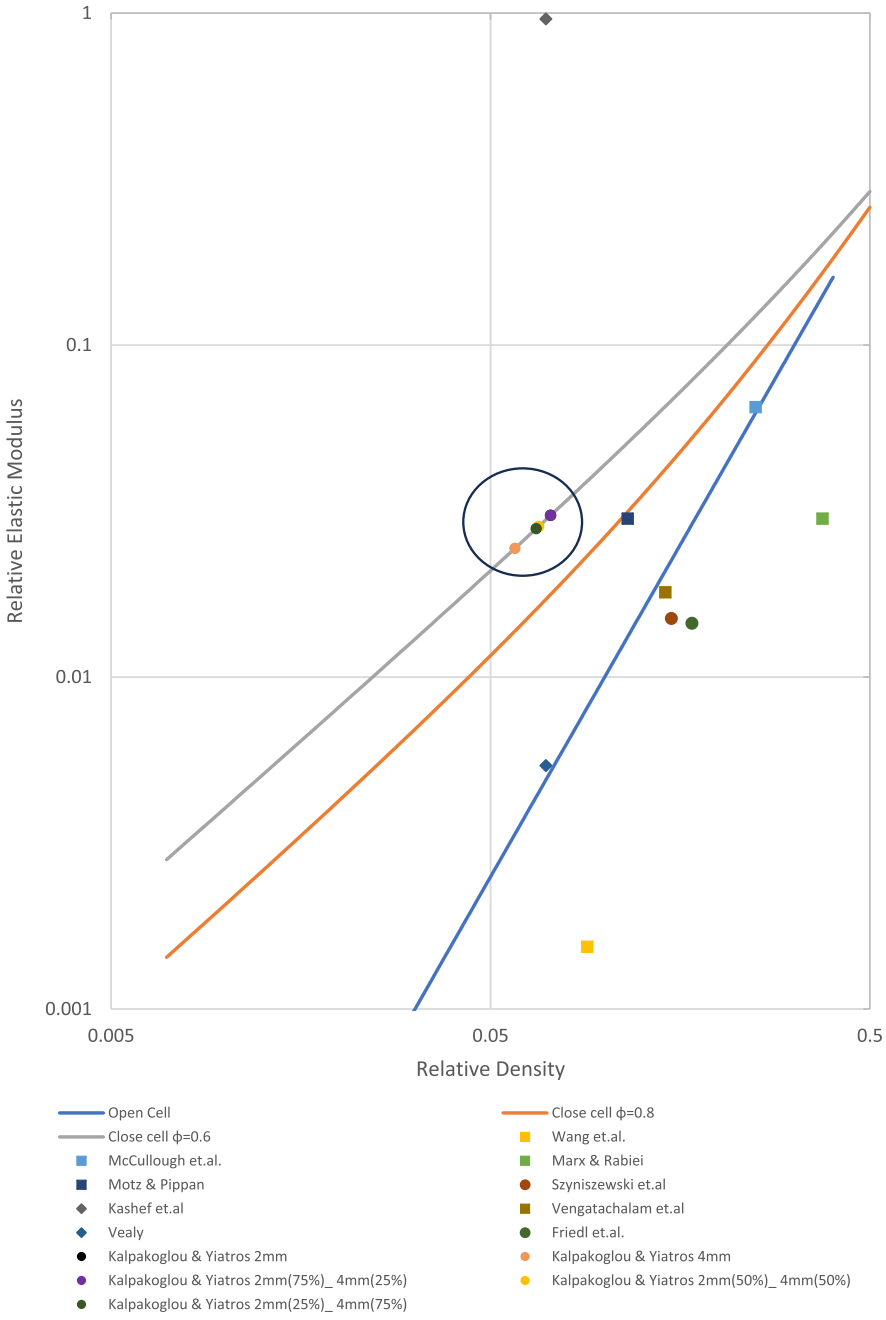

Fig. 24. Values obtained from the previous works and current for the Relative Elastic Modulus $\left(E/E_s\right)$ of foams against Relative Density $\left(\rho/\rho_s\right)$.Circles indicate hollow sphere foams, rhombuses indicate open-cell foams, and squares indicate closed-cell foams. The scale in both axes is logarithmic [95].

characteristics than the SHS4 specimens and, in some cases, even better than SHS2. One explanation is that the mixtures' packing creates more interconnected bonds within the assemblies, making tensile failure planes more complicated and, thus, more challenging for cracks to form. The increase in relative density, through an increase in the proportion of 2 mm spheres, increases Elastic Modulus and Tensile Strength values, with mean values closely matching the scaling curves by Gibson and Ashby[84].

The main objective of the present research was to develop a reliable method for determining the mechanical properties of metal foams in tension. One of the prerequisites for the reliability of the investigation method is matching experimental and theoretical values. This is achieved in Figs. 24 and 25, and is mainly linked to.

a) The shape of the specimens. The present research selected cubic specimens with minimal or zero machining with dimensions of at least 10 times the scale of constituent spheres, properly packed to ensure a representative volume.
b) The specimen preparation process preserves precise dimensions and mass, thus ensuring similar packing and relative density across each testing group.
c) The quality and strength of the adhesive joining the specimen to the grip tabs is much stiffer than that of the specimens, and the plane of failure within the specimen.
d) The low speed used during the experiment was 30 mm/h.

It will be interesting to repeat the experimental process with smaller

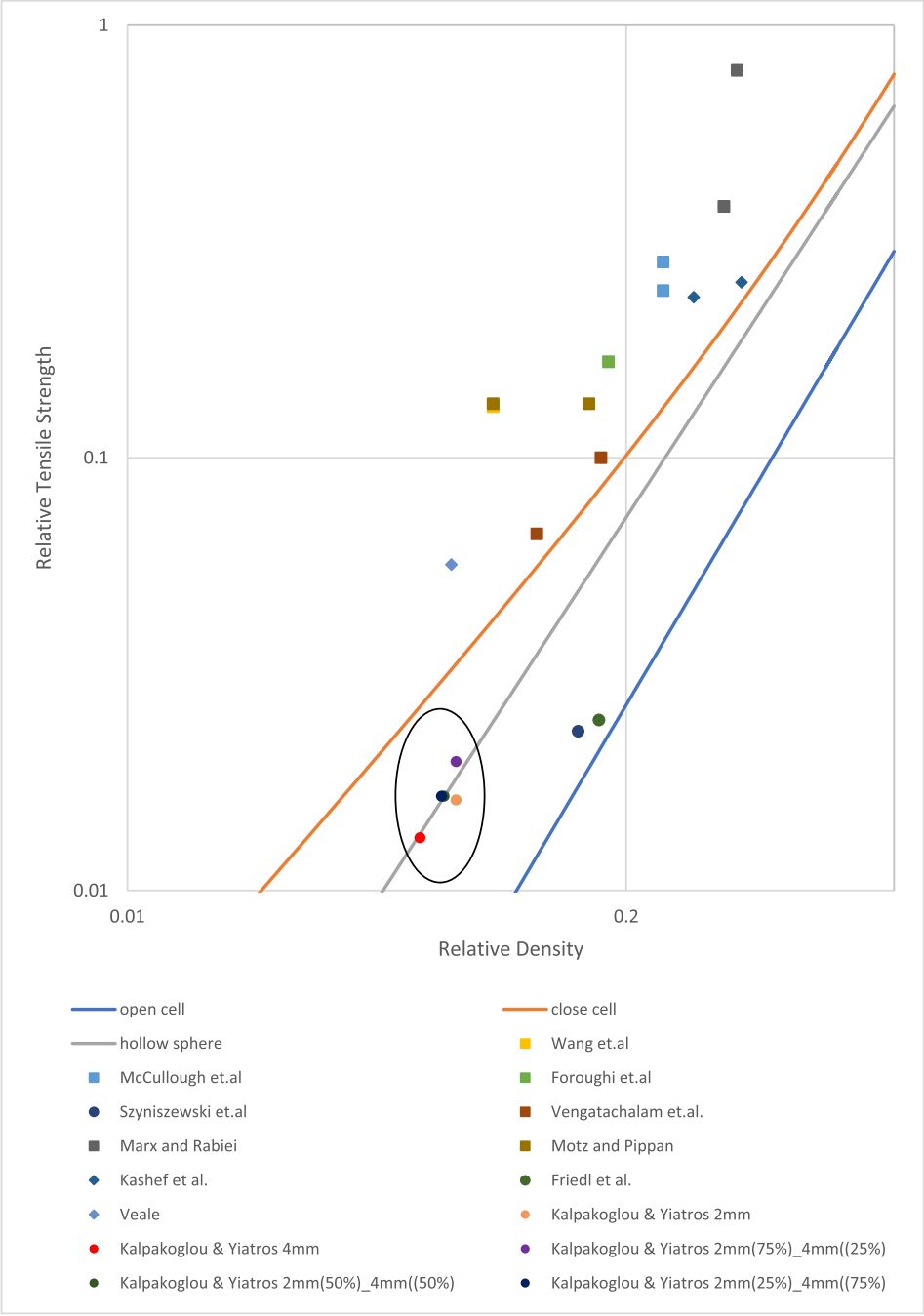

Fig. 25. Values obtained from the previous works and current for the Relative Tensile Strength $\left(\sigma_{max}/\sigma_{ys}\right)$ of foams against Relative Density $\left(\rho/\rho_s\right)$.Circles indicate hollow sphere foams, rhombuses indicate open-cell foams, and squares indicate closed-cell foams. The scale in both axes is logarithmic [95].

or larger specimens to confirm the present results. Previous attempts [83] in evaluating metal foam properties in tension used ASTM E8, the standard method of tensing metallic materials in tension. In this work, we used fixtures from testing flatwise bonding adhesives for composites in tension to cater for problems with the adhesion and transfer of load from the grips to the specimens. Flatwise adhesion and scale of the specimen dimensions (i.e., greater than 10 cells in each dimension) have shown potential merits for developing a standard method for metal foams.

Figs. 8 and 17 show that adding 2 mm spheres at 25 % to specimens where the main type of spheres is 4 mm increases the stress experienced by each specimen before fracture, which is connected to the various bonds that develop within the specimen. Something similar occurs where 4 mm spheres comprise 25 % of the total specimens, Figs. 7 and 15. Without, however, observing a significant difference in the number of bonds in the first case, and that does not apply in the second one, as the specimens consisting of two different types of spheres have a lower number of bonds, according to Table 13. Of course, it should be emphasised that the hybrid specimens with two types fractured in their middle third section show a better distribution of the load within the specimen.

In Fig. 15, specimens SHS2_0.75_SHS4_0.25(5) and SHS2_0.75_SHS4_0.25(6) exhibit initially a similar stiffness response with a mild deviation after the unloading-reloading cycle. This deviation

Table 13
The zone where the crack started per specimen.

Specimen	Zone 1–2 or 3-4	Zone 2-3
SHS2_075_SHS4_0,25(1)		X
SHS2_0,75_SHS4_0,25(2)		X
SHS2_0,75_SHS4_0,25(3)		X
SHS2_0,75_SHS4_0,25(5)		X
SHS2_0,75_SHS4_0,25(6)		X
SHS2_0,75_SHS4_0,25(10)		X
SHS2_0,50_SHS4_0,50(1)		X
SHS2_0,50_SHS4_0,50(3)		X
SHS2_0,50_SHS4_0,50(5)		X
SHS2_0,50_SHS4_0,50(6)		X
SHS2_0,50_SHS4_0,50(8)		X
SHS2_0,25_SHS4_0,75(1)		X
SHS2_0,25_SHS4_0,75(2)		X
SHS2_0,25_SHS4_0,75(3)		X
SHS2_0,25_SHS4_0,75(4)	X	
SHS2_0,25_SHS4_0,75(9)		X

Table 14
Number of bonds per type of specimen.

Specimen	Number of Bonds
SHS2	4350
SHS4	1952
SHS2_0,75_SHS4_0,25	2431
SHS2_0,5_SHS4_0,5	2740
SHS2_0,25_SHS4_0,75	2082

Comparing the number of bonds with Figs. 20 and 21, it is visible that it follows the present trend.

can be attributed to a potential earlier crack initiation in SHS2_0.75_SHS4_0.25(6), which led to the loss of the initial stiffness the two specimens exhibited, yielding a moderately softer response. According to the results obtained through the experimental process, it was shown that the increase in density has a more significant impact on improving the mechanical properties in proportion to the number of bonds, where it can be observed that it plays a minor role. For example, in Tables 6, 10 and 14, we observe that specimens with 75 % 2 mm spheres have properties similar to those with purely 2 mm spheres, but show a significant difference in the number of bonds that existed at the crack point. This can be explained through observations from previous research[83], according to which larger diameter spheres can potentially mitigate the failure of hollow spherical shells at the connection points with neighbouring spheres. Also, at this point, it is worth mentioning the statement of Sanders and Gibson[112] that there is an optimal welding angle for maximising the mechanical properties for a given relative shell thickness, t/R between spheres, which in the present case can be taken into account as a parameter which, however, cannot be controlled due to the randomness of the mixing of the spheres and

Table 15
Standard deviation and confidence interval data for the standard deviation of elastic modulus for each group of specimens.

Specimen	Number of specimens	Mean Value	Standard Deviation	Confidence Interval for the Standard Deviation (95.00 %)
SHS2	12	399,28	35,65	24,90-62,56
SHS4	9	340,89	53,88	36,39–103,22
SHS2_0,75_SHS4_0,25	6	387,58	24,86	15,52–60,96
SHS2_0,5_SHS4_0,5	5	383,58	37,20	22,29–106,88
SHS2_0,25_SHS4_0,75	5	344,84	37,65	22,55–108,18

Table 16
Standard deviation and confidence interval data for the standard deviation for tensile strength of each group of specimens.

Specimen	Number of specimens	Mean Value	Standard Deviation	Confidence Interval for the Standard Deviation (95.00 %)
SHS2	12	3,53	0,65	0,45-1,13
SHS4	9	2,80	0,69	0,47-1,33
SHS2_0,75_SHS4_0,25	6	4,17	0,27	0,17-0,66
SHS2_0,5_SHS4_0,5	5	3,47	0,73	0,43-2,10
SHS2_0,25_SHS4_0,75	5	3,47	0,53	0,32-1,52

Table 17
ANOVA table for elastic modulus.

Source of Variability	Sum of Squares (SSQ)	Degrees of Freedom(df)	Mean of SSQ	F-statistic	p-value
Variability Between Columns	22281,81	4	5570,44	2,73	0,04
Variability Within Columns	65308,6	32	2040,89		
Total	87590,4	36			

their connection during the preparation process of the samples. On the other hand, the increase in the relative density leads to a proportional increase in the mechanical properties (Tables 6–7,10-12).

Based on the results, it can be assumed that the thermosetting adhesive (Araldite AT1-1) plays an important role in the determination of the tensile strength of the specimens. Several factors can affect the performance of the adhesive, including its ageing since coating, storage conditions, coating thickness prior to curing, and the curing temperature. A stronger adhesive can shift the failure to the spherical shells,

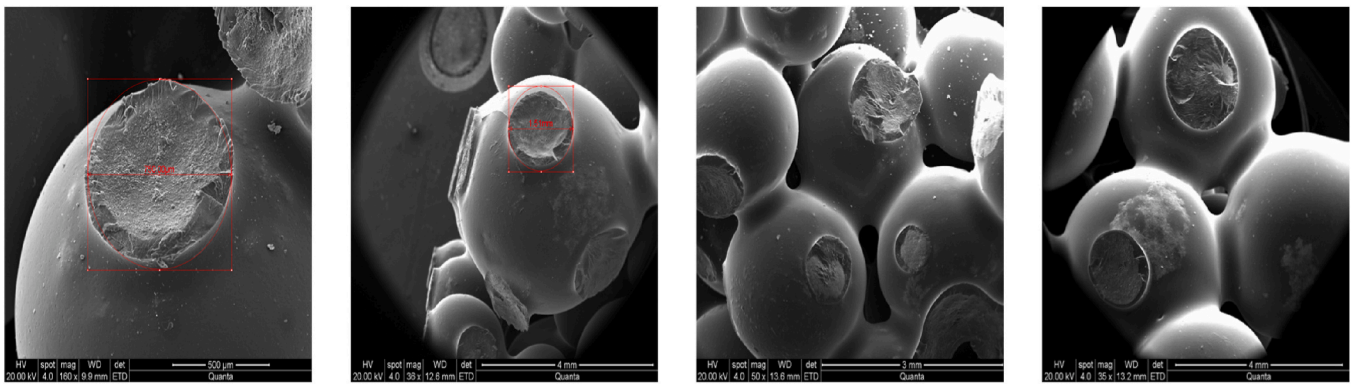

Fig. 26. Different cases of connections between spheres under the microscope.

Table 18
ANOVA table for tensile strength.

Source of Variability	Sum of Squares (SSQ)	Degrees of Freedom(df)	Mean of SSQ	F-statistic	p-value
Variability Between Columns	8,52	4	2,13	5,09	0,002
Variability Within Columns	13,4	32	0,41		
Total	21,92	36			

Table 19
Post-Hoc analysis for elastic modulus (ANOVA), where G1 is SHS2, G2 is SHS4, G3 is SHS2_0,75_SHS4_0,25, G4 is SHS2_0,5_SHS4_0,5, G5 is SHS2_0,25_SHS4_0,75.

Group 1	Group 2	Mean Difference	Lower Confidence Level	Upper Confidence Level	p-value
{'G1'}	{'G2'}	−1,40	56,16	113,72	0,06
{'G1'}	{'G3'}	−65,29	−0,03	65,24	1,00
{'G1'}	{'G4'}	−70,11	−0,63	68,85	1,00
{'G1'}	{'G5'}	−33,56	35,93	105,41	0,57
{'G2'}	{'G3'}	−124,99	−56,19	12,61	0,15
{'G2'}	{'G4'}	−129,60	−56,80	16,01	0,19
{'G2'}	{'G5'}	−93,05	−20,24	52,57	0,93
{'G3'}	{'G4'}	−79,65	−0,61	78,43	1,00
{'G3'}	{'G5'}	−43,09	35,95	114,99	0,68
{'G4'}	{'G5'}	−46,00	36,56	119,12	0,71

Table 20
Post-Hoc analysis for tensile strength (ANOVA), where G1 is SHS2, G2 is SHS4, G3 is SHS2_0,75_SHS4_0,25, G4 is SHS2_0,5_SHS4_0,5, G5 is SHS2_0,25_SHS4_0,75.

Group 1	Group 2	Mean Difference	Lower Confidence Level	Upper Confidence Level	p-value
{'G1'}	{'G3'}	−0,16	0,65	1,48	0,17
{'G1'}	{'G3'}	−1,76	−0,82	0,1	0,10
{'G1'}	{'G4'}	−1,24	−0,24	0,74	0,94
{'G1'}	{'G5'}	−1,23	−0,23	0,76	0,96
{'G2'}	{'G3'}	−2,47	−1,48	−0,49	0,001
{'G2'}	{'G4'}	−1,94	−0,90	0,13	0,11
{'G2'}	{'G5'}	−1,93	−0,89	0,15	0,12
{'G3'}	{'G4'}	−0,55	0,57	2	0,58
{'G3'}	{'G5'}	−0,53	0,59	2	0,56
{'G4'}	{'G5'}	−1,16	0,01	1	1,00

leading to stiffer elastic responses and potentially less brittle failure.

4. Conclusion

Although metal foams are attracting increasing attention, standardised testing procedures and reliable data regarding their tensile properties remain limited. This deficiency challenges accurate modelling and the secure design of components incorporating foams under tensile or combined loading. This issue arises due to the fact that the material at hand is both metallic and porous (foam) in nature. Previous work relied on testing methods for metals, which often led to inappropriate failures at the grip locations. This study seeks to address that shortfall, by considering the foam characteristics of the materials and exploring the potential of flatwise methods for investigating the tensile properties of steel foam sphere assemblies, by considering a setup used by standard EN 2243–4:2006 (CEN, 2020) for testing adhesives, and by using a sufficiently stiff and strong adhesive push the zone of failure into the steel foam hollow sphere assembly.

In the present research context, two distinct specimen groups with one sphere diameter type were used to capture the experimental methodology's suitability and efficacy. Once this was settled, the next step was to prepare and test hybrid specimen groups with different ratios of the two types of spheres in order to create specimen groups of different bulk density steel foam assemblies in the range between the two initial specimen groups. All experiments were done under displacement control with a 30 mm/h displacement rate using specialized grips. This investigation aims to contribute towards a model for studying mechanical properties (tensile strength and Elastic Modulus) under the effect of tensile loading, investigating the reliability of the method of specimen preparation and testing, as well as considering the effect of relative density as a design parameter for such steel foam sphere assemblies.

The new testing protocol exhibited promising results in terms of specimen preparation (specimen geometry, minor deviations in relative density), the high proportion of accepted testing failure responses, and mechanical properties (elastic modulus, tensile strength). Despite the minor deviations in the mechanical properties results, there is a very good alignment with the Gibson and Ashby [84] design curves, which was revealed in the present work and has not been presented in the past in other research. By establishing a strong connection between the tabs and the specimen via the selection of a high strength adhesive (tensile strength in excess of 35 MPa), the tests proceeded with failures occurring largely in the middle third of the specimens. Given the expected strength of metal foams and steel foam hollow sphere assemblies, the proposed test protocol yielded promising results for a relatively inexpensive method to test reliably the tensile strength of low relative density porous metals and metal foam sphere assemblies. The investigation proceeded with testing specimens groups of different relative density, reinforcing the protocol's reliability and generating more test data to create a design envelope. It is important to highlight, though, that the selected testing protocol can become a relatively inexpensive and accessible method to evaluate the tensile mechanical properties of low relative density porous metals and metal foam assemblies, further supporting practitioners in industrial uptake of the material.

A possible extension for this work is to enhance and better understand the results by using techniques such as X-ray tomography or EBSD to analyse internal defects, bonding quality, or grain orientation and using Energy Disruptive Spectroscopy or fracture surface analysis to assess bond ruptures. Through this, the effect of the bonds that develop between the spheres and their packing will be further examined, shedding light on the effects of relative density on the tensile mechanical properties and ensuing tensile failure. Finally, in a similar fashion, we will investigate the mechanical properties of metal foams under the effect of shear loading, where there is a gap in the predictability of both shear modulus and strength. The methodology for specimen preparation will follow the present methodology with adjustments for geometry. The test set up is based on the ASTM C393 [113], and the aim is to assess the viability and reliability of the method, including the adhesion to the grips and appropriate failure mechanisms, in order to fill the gap in the literature for reliable shear properties for low density metal foams.

CRediT authorship contribution statement

Thomas Kalpakoglou: Writing – review & editing, Writing – original draft, Visualisation, Methodology, Investigation, Formal analysis, Data curation, Conceptualisation. Georgios Constantinides: Writing – review & editing, Visualisation, Supervision. Stylianos Yiatros: Writing – review & editing, Supervision, Project administration.

Declaration of competing interest

The authors declare that they have no known competing financial interests or personal relationships that could have appeared to influence the work reported in this paper.

Acknowledgment

This research did not receive any specific grant from funding agencies in the public, commercial, or not-for-profit sectors.

Data availability

Data will be made available on request.

References

[1] Yiatros S, et al. Compressive properties of granular foams of adhesively bonded steel hollow sphere blocks. Mech Res Commun 2018;94:13–20. https://doi.org/10.1016/j.mechrescom.2018.08.005.
[2] Aly MS. Tensile properties of open-cell nickel foams. Mater Des 2010;31(4):2237–40. https://doi.org/10.1016/j.matdes.2009.10.018.
[3] Donghui Y, et al. Quasi-static compression deformation and energy absorption characteristics of basalt fiber-containing closed-cell aluminum foam. Metals 2020;10(7).
[4] Campana F, Mancini E, Daniela Pilone MS. Failure mechanisms of an Al 6061 alloy foam under dynamic conditions. Materials 2021;14(6):1–12. https://doi.org/10.3390/ma14061349. 2021.
[5] Nettey-oppong EE, et al. Mechanical properties and deformation behavior of equiatomic CoCrFeMnNi high-entropy alloy foam : a molecular dynamics study. Solid State Commun 2023;371(June):115236. https://doi.org/10.1016/j.ssc.2023.115236.
[6] Benedetti M, et al. Materials science & engineering R architected cellular materials : a review on their mechanical properties towards fatigue-tolerant design and fabrication. Mater Sci Eng R 2021;144:100606. https://doi.org/10.1016/j.mser.2021.100606.
[7] Ates M, et al. 'Polyurethane foam materials and their industrial applications', 2022(August). https://doi.org/10.1002/pi.6441; 2022.
[8] Mohammed HI. Discharge improvement of a phase change material - air - based thermal energy storage unit for space heating applications using metal foams in the air sides. Heat Transfer 2022;51(5):3830–52. https://doi.org/10.1002/htj.22479.
[9] Sharma SS, et al. Materials today : Proceedings application of metallic foam in vehicle structure : a review. Mater Today Proc 2022;63:347–53. https://doi.org/10.1016/j.matpr.2022.03.201.
[10] Buonomo B, et al. Performance parameters enhancement of a thermoelectric generator by metal foam in exhaust automotive lines. Therm Sci Eng Prog 2023;38(December 2022):101684. https://doi.org/10.1016/j.tsep.2023.101684.
[11] Castañeda-rodríguez S, González-torres M, Ribas-aparicio RM. Recent advances in modified poly (lactic acid) as tissue engineering materials. J Biol Eng 2023;8:1–20.
[12] Tyagi SA, Manjaiah M. Bioprinting additive manufacturing of titanium-based lattice structures for medical applications – a review. Bioprinting 2023;30(March):e00267. https://doi.org/10.1016/j.bprint.2023.e00267.
[13] Bienvenu Y. Application and future of solid foams. C R Phys 2014;15(8–9):719–30. https://doi.org/10.1016/J.CRHY.2014.09.006/.
[14] Bedell M, et al. A case for closed-loop recycling of post-consumer PET for automotive foams. Waste Manag 2018;71:97–108. https://doi.org/10.1016/j.wasman.2017.10.021.
[15] Bisht A, Patel VK, Gangil B. Future of metal foam materials in automotive industry. In: Energy Environment, and Sustainability; 2019. p. 51–63. https://doi.org/10.1007/978-981-15-0434-1_4/FIGURES/8.
[16] Salins SS, et al. Characterization of the aluminium-based metal foam properties for automotive applications. Arabian J Sci Eng 2024:1–14. https://doi.org/10.1007/S13369-024-09399-3/FIGURES/10.
[17] Banhart J, Schmoll C, Neumann U. Light-weight aluminium foam structures for ships. In: Proc. Conf. Materials in Oceanic Environment; 1998. p. 55–63. 1 (August).
[18] Crupi V, Epasto G, Guglielmino E. Impact response of aluminum foam sandwiches for light-weight ship structures. Metals 2011;1(1):98–112. https://doi.org/10.3390/MET1010098. 2011, Vol. 1, Pages 98-112.
[19] Murugesan G, Mansuri H. Experimental study of composite foam sandwich structures for aerospace applications structural dynamic analysis of turbine blade view project experimental study of composite foam sandwich structures for aerospace applications. SSRG International Journal of Mechanical Engineering (SSRG-IJME), 5, https://doi.org/10.14445/23488360/IJME-V5I3P104; 2018.
[20] Zhu L, Li N, Childs PRN. Light-weighting in aerospace component and system design. Propuls Power Res 2018;7(2):103–19. https://doi.org/10.1016/J.JPPR.2018.04.001.
[21] Ensarioglu Cihat, et al. Metal foams and their applications in aerospace components. Cham: Springer; 2022. p. 27–63. https://doi.org/10.1007/978-3-030-91873-6_2.
[22] Wang G, et al. Heat transfer characteristics of flat-plate micro heat pipes with integrated copper foam for aerospace thermal management. Appl Therm Eng 2025;263:125319. https://doi.org/10.1016/J.APPLTHERMALENG.2024.125319.
[23] Sajid Hossain M, Shabani B. Metal foams application to enhance cooling of open cathode polymer electrolyte membrane fuel cells. J Power Sources 2015;295:275–91. https://doi.org/10.1016/j.jpowsour.2015.07.022.
[24] Allioux FM, et al. Catalytic metal foam by chemical melting and sintering of liquid metal nanoparticles. Adv Funct Mater 2020;30(5):1907879. https://doi.org/10.1002/ADFM.201907879.
[25] Du R, et al. Engineering self-supported noble metal foams toward electrocatalysis and beyond. Adv Energy Mater 2020;10(11):1901945. https://doi.org/10.1002/AENM.201901945.
[26] Hu Y, et al. Metal coordination assists fabrication of multifunctional aerogel. J Mater Sci Technol 2021;71:67–74. https://doi.org/10.1016/j.jmst.2020.09.007.
[27] Chen C, et al. δ-MnO2 decorated layered double oxides in-situ grown on nickel foam towards electrothermal catalysis of n-heptane. J Environ Sci 2023;126:308–20. https://doi.org/10.1016/J.JES.2022.03.017.
[28] Salimon A, et al. Potential applications for steel and titanium metal foams. J Mater Sci 2005;40(22):5793–9. https://doi.org/10.1007/s10853-005-4993-x.
[29] Bisht A, Patel VK, Gangil B. Future of metal foam materials in automotive industry. In: Jitendra Kumar Katiyar VK, Bhattacharya Shantanu, Kumar Patel Vinay, editors. Energy, environment, and sustainability. Singapore: Springer Nature; 2019. p. 51–63. https://doi.org/10.1007/978-981-15-0434-1_4/COVER. 152 Beach Road, Gateway East, Singapore 189721.
[30] Farhadi S, Kafili D, Ziadloo S. Review of aluminum foam applications in architecture. Europ J Eng Sci Technol 2020;3(1):62–70. https://doi.org/10.33422/EJEST.V3I1.162.
[31] Chibani A, Merouani S, Benmoussa F. Computational analysis of the melting process of phase change material-metal foam-based latent thermal energy storage unit: the heat exchanger configuration. J Energy Storage 2021;42:103071. https://doi.org/10.1016/J.EST.2021.103071.
[32] Song J, et al. Energy-absorption behavior of metallic hollow sphere structures under impact loading. Eng Struct 2021;226(August 2020):111350. https://doi.org/10.1016/j.engstruct.2020.111350.
[33] Ghalambaz M, et al. Improving phase change heat transfer in an enclosure partially filled by uniform and anisotropic metal foam layers. Int J Heat Mass Tran 2024;228:125678. https://doi.org/10.1016/J.IJHEATMASSTRANSFER.2024.125678.
[34] Liu Y, et al. Foam concrete for lightweight construction applications: a comprehensive review of the research development and material characteristics. Rev Adv Mater Sci 2024;63(1). https://doi.org/10.1515/RAMS-2024-0022/ASSET/GRAPHIC/J_RAMS-2024-0022_FIG_011.JPG.
[35] Lafdi K, Mesalhy O, Elgafy A. Graphite foams infiltrated with phase change materials as alternative materials for space and terrestrial thermal energy storage applications. Carbon 2008;46(1):159–68. https://doi.org/10.1016/J.CARBON.2007.11.003.
[36] Huang X, et al. Shape-stabilized phase change materials based on porous supports for thermal energy storage applications. Chem Eng J 2019;356:641–61. https://doi.org/10.1016/J.CEJ.2018.09.013.
[37] Lei J, et al. Heat transfer enhancement in latent heat thermal energy storage using copper foams with varying porosity. Sol Energy 2021;221:75–86. https://doi.org/10.1016/J.SOLENER.2021.04.013.
[38] Galvagnini F, Valentini F, Dorigato A. Development of polymeric insulating foams for low-temperature thermal energy storage applications. J Appl Polym Sci 2022;139(25):e52397. https://doi.org/10.1002/APP.52397.
[39] Mert HH, et al. Development of composite phase change materials based on n-tetradecane and β-myrcene based foams for cold thermal energy storage applications. Thermochim Acta 2022;707:179116. https://doi.org/10.1016/J.TCA.2021.179116.
[40] Merolli A, Joyce TJ. Biomaterials in hand surgery, biomaterials in hand surgery. Milan: Springer; 2009. https://doi.org/10.1007/978-88-470-1195-3.
[41] Patel P, Bhingole PP, Makwana D. Manufacturing, characterization and applications of lightweight metallic foams for structural applications: review. Mater Today Proc 2018;5(9):20391–402. https://doi.org/10.1016/j.matpr.2018.06.414.
[42] Tong X, et al. Degradation behavior, cytotoxicity, hemolysis, and antibacterial properties of electro-deposited Zn–Cu metal foams as potential biodegradable bone implants. Acta Biomater 2020;102:481–92. https://doi.org/10.1016/J.ACTBIO.2019.11.031.
[43] Rodriguez-Contreras A, et al. Powder metallurgy with space holder for porous titanium implants: a review. J Mater Sci Technol 2021;76:129–49. https://doi.org/10.1016/j.jmst.2020.11.005.
[44] Madgule M, et al. Influence of foaming agents on mechanical and microstructure characterization of AA6061 metal foams. Proc Inst Mech Eng Part E J Process Mech Eng 2024;238(2):520–32. https://doi.org/10.1177/09544089221097534/SUPPL_FILE/SJ-DOCX-1-PIE-10.1177_09544089221097534.DOCX.
[45] Abdel-Karim R. Recent advancements in nanoporous metal foams for biomedical applications: processing and mechanical properties. In: Metals in medicine. New York: Apple Academic Press; 2025. p. 1–40. https://doi.org/10.1201/9781003538189-1.
[46] Yadav D, et al. Metallic foams for biomedical application. In: Metals in medicine. New York: Apple Academic Press; 2025. p. 85–100. https://doi.org/10.1201/9781003538189-4.
[47] Çakır ÖF, Erdem M. Investigation of lattice geometries formed by metal powder additive manufacturing for energy absorption: a comparative Study on Ti6Al4V, inconel 718, and AISI 316L. Machines 2025;vol. 13. https://doi.org/10.3390/MACHINES13040316. 4.
[48] Hirankittiwong P, et al. Advanced engineered nanostructures for aerospace technology: a review. Results Eng 2025;26. https://doi.org/10.1016/J.RINENG.2025.105381.

[49] Zarei F, Shafiei-Zarghani A. Inhomogeneous schwarz diamond lattice structures for load-bearing orthopedic implants: fabrication and mechanical evaluation. Iran J Sci Technol Transact Mech Eng 2025;49(3):1361–75. https://doi.org/10.1007/S40997-025-00844-8.
[50] Siyao M, et al. Functional investigation on automotive interior materials based on variable knitted structural parameters. Polymers 2020;12(11):2455. https://doi.org/10.3390/POLYM12112455. Page 2455, 12.
[51] Li B, et al. Effects of tensile and compressive stress on bone resorption and formation parameters surrounding dental implants. J Mech Behav Biomed Mater 2025;165:106928. https://doi.org/10.1016/J.JMBBM.2025.106928.
[52] Valeri P, Fernàndez Ruiz M, Muttoni A. Tensile response of textile reinforced concrete. Constr Build Mater 2020;258:119517. https://doi.org/10.1016/J.CONBUILDMAT.2020.119517.
[53] Chen C, Harte AM, Fleck NA. The plastic collapse of sandwich beams with a metallic foam core. Int J Mech Sci 2001;43(6):1483–506. https://doi.org/10.1016/S0020-7403(00)00069-2.
[54] Guo J, et al. Compression effect of metal foam on melting phase change in a shell-and-tube unit. Appl Therm Eng 2022;206(January):118124. https://doi.org/10.1016/j.applthermaleng.2022.118124.
[55] Kertész J, et al. Al-Foam compression tests in parallel and serial concepts. Appl Sci 2023;13(2):1–14. https://doi.org/10.3390/app13020883.
[56] Ramamurty U, Paul A. Variability in mechanical properties of a metal foam. Acta Mater 2004;52:869–76. https://doi.org/10.1016/j.actamat.2003.10.021.
[57] Grilec K, Maric G, Jakovljević Suzana. A study on energy absorption of aluminium foam. BHM Berg- Hüttenmännische Monatsh 2010;155(April). https://doi.org/10.1007/s00501-010-0567-6.
[58] Venkata B, Dinesh S, Bhattacharya A. Comparison of energy absorption characteristics of PCM-metal foam systems with different pore size distributions. J Energy Storage 2020;28(December 2019). https://doi.org/10.1016/j.est.2019.101190.
[59] Weise J, et al. Production and properties of 316L stainless steel cellular materials and syntactic foams. Steel Res Int 2014;85(3):486–97. https://doi.org/10.1002/srin.201300131.
[60] Yiatros S, et al. Institution of structural engineers research fund experimental investigation of vibration damping in steel foam sandwich institution of structural engineers research fund. 2017. p. 3–6.
[61] Tavares M, et al. 'International journal of mechanical sciences mechanical behavior of steel and aluminum foams at elevated temperatures. In: Local buckling based approach toward understanding of the material system behavior; 2020. https://doi.org/10.1016/j.ijmecsci.2020.105754. 181(May).
[62] Novak N, et al. Experimental and computational evaluation of tensile properties of additively manufactured hexa- and tetrachiral auxetic cellular structures. Addit Manuf 2021;45(April). https://doi.org/10.1016/j.addma.2021.102022.
[63] Mei Y, et al. Tensile behavior and performance of syntactic steel foams prepared by infiltration casting. Metals 2022;12(4):1–14. https://doi.org/10.3390/met12040668.
[64] Pelleg J. Mechanical properties of materials. New York London: Springer; 2013. https://doi.org/10.1007/978-94-007-4342-7. Dordrecht.
[65] Surjadi JU, et al. Mechanical metamaterials and their engineering applications. https://doi.org/10.1002/adem.201800864; 2019.
[66] Qi C, Jiang F, Yang S. Advanced honeycomb designs for improving mechanical properties : a review. Composites Part B 2021;227(August):109393. https://doi.org/10.1016/j.compositesb.2021.109393.
[67] Lefebvre BL, Banhart J, Dunand DC. Porous metals and metallic foams : current status and recent developments. Adv Eng Mater 2008;10(9):775–87. https://doi.org/10.1002/adem.200800241.
[68] Jiang B, et al. Ultralight metal foams. Nature Publishing Group; 2015. p. 1–8. https://doi.org/10.1038/srep13825.
[69] Madgule M, Sreenivasa CG, Borgaonkar AV. Materials today : Proceedings aluminium metal foam production methods , properties and applications- a review. Mater Today Proc 2023;77:673–9. https://doi.org/10.1016/j.matpr.2022.11.287.
[70] Sehrawat R, Kumar R, Sumit S. Heat storage material : a hope in solar thermal. Environ Sci Pollut Control Ser 2023:11175–98. https://doi.org/10.1007/s11356-022-24552-x.
[71] Hassan A, Alnaser IA. A review of different manufacturing methods of metallic foams. ACS Omega 2024;9(6):6280–95. https://doi.org/10.1021/ACSOMEGA.3C08613/ASSET/IMAGES/LARGE/AO3C08613_0016.JPEG.
[72] Xing M, et al. Enhanced solidification/melting heat transfer process by multiple copper metal foam for ice thermal energy storage. J Energy Storage 2024;79:110207. https://doi.org/10.1016/J.EST.2023.110207.
[73] Angelo PC, Subramanian R, Angelo PC, Subramanian R. Powder metallurgy: science, technology and applications. 1st edn. New Delhi: PHI Learning Private Limited; 2008. 1st edn. New Delhi SE -: PHI Learning Private Limited New Delhi. Available at: https://doi.org/LK-https://worldcat.org/title/769047654.
[74] Guerrero CT, et al. A study on syntactic aluminum foams manufactured infiltrating sintered preforms of iron hollow spheres. Mater Chem Phys 2024;323:129656. https://doi.org/10.1016/J.MATCHEMPHYS.2024.129656.
[75] Zewdie F, et al. Experimental investigation on fabrication of cermet hollow spheres for use as reinforcement in the production of lightweight and strong metal foams for high energy absorption applications. J Mater Eng Perform 2024:1–18. https://doi.org/10.1007/S11665-024-09339-0/FIGURES/12.
[76] Andersen BO, et al. Novel metallic hollow sphere structures. Adv Eng Mater 2000;2(4):192–5.
[77] Miądlicki P, Rychtowski P, Tryba B. Coating of expanded polystyrene spheres by TiO2 and SiO2–TiO2 thin films. J Mater Res 2024;39(10):1473–88. https://doi.org/10.1557/S43578-024-01319-3/FIGURES/10.
[78] Lim T, Smith B, Mcdowell DL. Behavior of a random hollow sphere metal foam. Acta Mater 2002;50:2867–79.
[79] Augustin C, Hungerbach W. Production of hollow spheres (HS) and hollow sphere structures (HSS). Mater Lett 2009;63(13–14):1109–12. https://doi.org/10.1016/j.matlet.2009.01.015.
[80] Goehler BH, et al. Functionalized metallic hollow sphere structures. 2014. p. 335–9. https://doi.org/10.1002/adem.201300057. 3.
[81] Jiang Z, et al. Contrasting effects of various factors upon the properties of foam ceramics and the mechanisms of crystalline phase reconstruction and microstructure regulation. Ceram Int 2024;50(12):21645–57. https://doi.org/10.1016/J.CERAMINT.2024.03.277.
[82] Friedl O, et al. Experimental investigation of mechanical properties of metallic hollow sphere structures. Metall Mater Trans B 2008;39(1):135–46. https://doi.org/10.1007/S11663-007-9098-2/FIGURES/14.
[83] Szyniszewski ST, et al. The mechanical properties and modeling of a sintered hollow sphere steel foam. Mater Des 2014;54:1083–94. https://doi.org/10.1016/j.matdes.2013.08.045.
[84] Gibson LJ, Ashby MF. Cellular solids: structure and properties, second edition, cellular solids: structure and properties, second edition. Cambridge University Press; 1997. https://doi.org/10.1017/CBO9781139878326.
[85] Zimar AMZ, et al. Non-linear behaviour of open-cell metal foam under tensile loading. In: 2nd international moratuwa engineering research conference, MERCon 2016; 2016. p. 349–54. https://doi.org/10.1109/MERCON.2016.7480166.
[86] Foroughi B, Degischer HP, Kottar A. Characterization and simulation of tensile deformation of non-uniform cellular aluminium until damage. Adv Eng Mater 2013;15(4):276–86. https://doi.org/10.1002/adem.201200163.
[87] Marx J, Rabiei A. Tensile properties of composite metal foam and composite metal foam core sandwich panels. J Sandw Struct Mater 2020. https://doi.org/10.1177/1099636220942880 [Preprint].
[88] Vengatachalam B, et al. Initial yield behaviour of closed-cell aluminium foams in biaxial loading. Int J Mech Sci 2021;191(September 2020):106063. https://doi.org/10.1016/j.ijmecsci.2020.106063.
[89] Qing HB, Liu PS, Xu XB. Primary investigation on an iron foam sandwich structure. Met Mater Int 2020:610–7. https://doi.org/10.1007/s12540-020-00830-6. May 2020.
[90] Bolzoni L, Carson JK, Yang F. Combinatorial structural-analytical models for the prediction of the mechanical behaviour of isotropic porous pure metals. Acta Mater 2021;207(January):116664. https://doi.org/10.1016/j.actamat.2021.116664.
[91] McCullough KYG, Fleck NA, Ashby MF. Uniaxial stress-strain behaviour of aluminum alloy foams. Acta Mater 1999;47(8):2323–30. https://doi.org/10.1016/S1359-6454(99)00128-7.
[92] McCullough KYG, Fleck NA, Ashby MF. Toughness of aluminum alloy foams. Acta Mater 1999;47(8):2331–43. https://doi.org/10.1016/S1359-6454(99)00125-1.
[93] Motz C, Pippan R. Deformation behaviour of closed-cell aluminium foams in tension. Acta Mater 2001;49(13):2463–70. https://doi.org/10.1016/S1359-6454(01)00152-5.
[94] Wang, et al. Tensile and shear properties of aluminium foam. Mater Technol 2009;24(3):161–5. https://doi.org/10.1179/106678509X12475884746705.
[95] Kalpakoglou T, Yiatros S. Metal foams : a review for mechanical properties under tensile and shear stress. 2022. p. 1–18. https://doi.org/10.3389/fmats.2022.998673. October.
[96] Kashef S, et al. Fracture toughness of titanium foams for medical applications. Mater Sci Eng 2010;527(29–30):7689–93. https://doi.org/10.1016/j.msea.2010.08.044.
[97] Vengatachalam B, et al. Initial yield behaviour of closed-cell aluminium foams in biaxial loading. Int J Mech Sci 2021;191(May 2020):106063. https://doi.org/10.1016/j.ijmecsci.2020.106063.
[98] Veale PJ. Investigation of the behavior of open cell aluminum foam, open cell aluminum foam. Amherst: University of Massachusetts; 2010. https://scholarworks.umass.edu/theses/443.
[99] Jung A, Diebels S. Micromechanical characterization of metal foams. Adv Eng Mater 2019;21(8):1900237. https://doi.org/10.1002/ADEM.201900237.
[100] Huang Minghao, et al. Optimizing crack initiation energy in austenitic steel via controlled martensitic transformation. J Mater Sci Technol 2024;198:231–42. https://doi.org/10.1016/J.JMST.2024.02.019.
[101] ASTM-C297. ASTM-C297-C297M-04-flatwise_tensile_strength_of_sandwich_constructions.pdf. Annu Book ASTM (Am Soc Test Mater) Stand 2010. ASTM Volum.
[102] ASTM-D3354. D3354 − 21 Standard Test Method for Blocking Load of Plastic Film by the Parallel Plate Method, 08(Reapproved 1989). pp. 3–4, https://doi.org/10.1520/C1709-18; 2021.
[103] ASTM D1623 − 17. 'D1623 − 17 standard test method for tensile and tensile adhesion properties of rigid cellular plastics', i(Reapproved). 3–5, https://doi.org/10.1520/D1623-17R23.2; 2017.
[104] EN 1607 : 2013. BS EN 1607 : 2013 BSI standards publication thermal insulating products for building applications — determination of tensile strength perpendicular to faces. 2013.
[105] EN 2243-4:2006. Non-metallic materials structural adhesives - test method - part 4: metal-honeycomb core flatwise tensile test 2020;1(I):2–5.
[106] Soboyejo W. Mechanical properties of engineered materials. first ed. York, New Basel: CRC Press; 2002. https://doi.org/10.1201/9780203910399.

[107] Goodno BJ, Gere JM. Mechanics of materials. ninth ed. Cengage; 2021. https://books.google.com/books/about/Mechanics_of_Materials.html?hl=el&id=rlVCxwEACAAJ. [Accessed 23 February 2024].
[108] Bohnenkamp U, Sandström R. Evaluation of the density of steels. Steel Res 2000; 71(3):88–93. https://doi.org/10.1002/SRIN.200005695.
[109] Nečas D, Klapetek P. Gwyddion: an open-source software for SPM data analysis. Cent Eur J Phys 2012;10(1):181–8. https://doi.org/10.2478/S11534-011-0096-2/MACHINEREADABLECITATION/RIS.
[110] Volaufova J. Heteroscedastic ANOVA: old p values, new views. Stat Pap 2009;50 (4):943–62. https://doi.org/10.1007/S00362-009-0262-4/METRICS.
[111] Kim H-Y. Statistical notes for clinical researchers: post-hoc multiple comparisons. Restorat Dentis Endodon 2015;40(2):172. https://doi.org/10.5395/RDE.2015.40.2.172.
[112] Sanders WS, Gibson LJ. Mechanics of hollow sphere foams. Mater Sci Eng, A 2003;347(1–2):70–85. https://doi.org/10.1016/S0921-5093(02)00583-X.
[113] ASTM-C393-C393M-06. ASTM-C393-C393M-06-Core_shear_properties_of_sandwich_constructions_by_beam_flexure. pdf`; 2006.